A cysteine-rich domain of the *Cryptococcus neoformans* Cuf1 transcription factor is required for high copper stress sensing and fungal virulence

Corinna Probst [1], Chloe Insler [1], Catherine A. Denning-Jannace [7], Estefany Y Reyes [4], Jonathan L Messerschmidt [4], Lukas M. du Plooy [8], Charles Giamberardino [1], Connie B. Nichols [1], Yohannes Asfaw [6], Mari L Shinohara [2,3,4], Katherine J. Franz [5], J. Andrew Alspaugh [1,2,3*]

Duke University School of Medicine, Durham, NC, USA: Departments of Medicine [1], Molecular Genetics and Microbiology [2], Cell Biology [3] and Integrative Immunobiology [4]

Duke University, Durham, NC, USA: Department of Chemistry [5]

Duke University, Durham, NC: Division of Laboratory Animal Resources [6]

University of North Carolina, Greensboro, USA, Department of Chemistry and Biochemistry[7]

University of Exeter, Exeter, UK, MRC Centre for Medical Mycology[8]

Running title: **High copper sensing in the human fungal pathogen *Cryptococcus neoformans***

Keywords: **nutritional immunity, metal homeostasis, fungal pathogenesis**

(*) Corresponding Author: J. Andrew Alspaugh, andrew.alspaugh@duke.edu

Abstract

The ability to sense, import and detoxify copper (Cu) has been shown to be crucial for microbial pathogens to survive within an infected host. Previous studies conducted with the opportunistic human fungal pathogen *Cryptococcus neoformans* (*Cn*) have revealed two extreme Cu environments encountered during infection: a high Cu environment within the lung and a low Cu environment within the brain. However, how *Cn* senses these different host Cu microenvironments, and the consequences of a blunted Cu stress adaptation for pathogenesis are not well understood. In contrast to ascomycete model fungi, the basidiomycete *Cn* has a single transcription factor (TF), *Cn*Cuf1, to regulate adaptive responses to both high- and low- Cu stress. Sequence comparison with other fungal Cu-responsive TFs identified three conserved cysteine (Cys)-rich motifs located within the *Cn*Cuf1 N-terminal domain, which were therefore predicted to play a role in Cu sensing. Mutation of these conserved Cys-rich motifs demonstrated that the 1st Cys-rich motif is functionally relevant for *Cn*Cuf1 transcriptional activity during high Cu stress, while it is dispensable for low Cu stress adaptation. An inhalation model of murine infection showed that strains with defective high Cu stress regulation present a distinct and anatomically constrained pattern of yeast distribution within the infected lungs compared to a more widespread infection observed in lungs infected with the wild-type strain. Based on these findings, we hypothesize that Cuf1-driven high Cu responses modulate not absolute fitness but containment of *Cn* cells at the initial site of infection within the lung.

Importance

Copper is an essential micronutrient required for survival in all kingdoms of life as it is used as a catalytic cofactor for many essential processes in the cell. In turn, this reactivity of copper ions makes elevated levels of free copper toxic for the cell. This dual nature of copper – essential for life but toxic at

elevated levels – is used by our innate immune system in a process called nutritional immunity to combat and kill invading pathogens. In this work we explore how the fungal human pathogen *Cryptococcus neoformans* senses high copper stress, a copper microenvironment encountered within the host lung. We identified a specific cysteine-rich motif within the copper responsive transcription factor Cuf1 to be essential for high copper stress sensing. Mutation of this motif led to an impaired high copper stress adaptation, which did not affect fitness of the yeast but did impact containment and distribution of yeast cells inside the host lung.

Introduction

Copper (Cu) is an essential trace element in both microbes and mammalian cells, serving as a catalytic cofactor for a diverse range of cellular processes including iron (Fe) uptake and distribution; mitochondrial cytochrome oxidase activity; Cu, Zinc (Zn) superoxide dismutase catalysis; and melanin pigment production [1, 2]. Although Cu is required for life, elevated Cu levels are toxic due to its ability to induce uncontrolled redox cycling, causing the formation of toxic reactive oxygen species (ROS) and oxidative damage of DNA, proteins, and lipids [3, 4]. Free Cu ions were also shown to induce protein aggregation, triggering protein misfolding and precipitation [5, 6]. Furthermore, Cu has been shown to irreversibly displace Fe from Fe-S-cluster containing proteins, rendering these proteins nonfunctional [7, 8]. Therefore, organisms have evolved processes to sense and tightly regulate cellular Cu availability to maintain but not exceed the required cellular Cu quota [2, 4, 9-11].

Pathogenic microbes encounter unique extremes of Cu stress. Infected hosts often employ Cu-sequestering strategies known as “nutritional immunity” to limit Cu availability for invading pathogens [12-17]. In other sites, such as the macrophage phagolysosome, the host ATP7A Cu pump actively imports Cu to toxic concentrations to kill engulfed microorganisms [18]. In contrast, recent

66 investigations demonstrated that brain resident microglia actually provide permissive conditions for the
67 persistence of a microbial pathogen in the central nervous system (CNS) by supplying Cu in this
68 otherwise nutritionally depleted site [13].

69 *Cryptococcus neoformans* (*Cn*) is an opportunistic fungal pathogen that causes life-threatening
70 disease in immune compromised individuals [19, 20]. *Cn* is a free-living environmental fungus,
71 frequently isolated from decaying plants, and soil contaminated with bird guano. Infectious spores or
72 desiccated yeast cells are inhaled by mammalian hosts from the environment, resulting in an initial
73 pulmonary infection [20]. In patients with weakened immune systems, including those with late-stage
74 HIV infection, *Cn* disseminates through the bloodstream, crosses the blood-brain barrier, and colonizes
75 the brain where it causes lethal infection [19, 20]. Previous studies have revealed that *Cn* encounters
76 two extreme Cu environments during infection. During the initial infection within the lung, *Cn* senses a
77 high Cu environment. In contrast, once the microorganism reaches the CNS, it senses low Cu availability
78 [21, 22]. Thus, to maintain proper cellular Cu homeostasis, *Cn* needs to switch from Cu-detoxification
79 during pulmonary infection to Cu-acquisition upon entering the CNS.

80 Several adaptive strategies for *Cn* Cu homeostasis have been described. To combat high Cu stress, *Cn*
81 induces the Cu-detoxifying metallothionein genes *CMT1* and *CMT2*, the ROS detoxifying superoxide
82 dismutase (*SOD*) 1 gene, as well as *ATM1,* a gene encoding a mitochondrial ABC transporter required to
83 provide a sulfuric precursor for cytosolic Fe-S cluster biosynthesis [23]. These genes were previously
84 shown to be required for *Cn* survival inside macrophages or in a mouse model of *cryptococcosis* [21, 24-
85 26]. In contrast, within the Cu-restricted CNS environment, *Cn* induces the expression of its two high
86 affinity copper importer genes, *CTR1* and *CTR4*, as well as the *CBI1* gene, encoding a Cu-binding protein
87 required for efficient Cu acquisition [22, 27, 28]. Additionally, recent investigations defined a tightly
88 regulated cellular switch between the Cu/Zn-dependent Sod1 to the Cu-independent/ manganese (Mn)-
89 dependent Sod2 during Cu limiting conditions. This switch allows the fungal cell to prioritize Cu for use

90 in other essential Cu-dependent cellular processes when labile Cu is limited without disturbing
91 intracellular ROS detoxification [11].

92 Cu sensing and regulation has been well studied in ascomycete model fungi, of which most employ
93 two distinct transcription factors (TFs) to control responses to high and low Cu stress [2]. For example,
94 the *Saccharomyces cerevisiae* (*Sc*) Ace1 transcription factor is activated in a high Cu environment to
95 regulate gene expression to protect the yeast from toxic Cu levels [29, 30], and the *Sc* Mac1
96 transcription factor is activated by low Cu environments to favor Cu acquisition [31]. In contrast, the
97 basidiomycete *Cn* maintains a single Cu-responsive transcription factor, Cuf1, that controls both high
98 and low Cu stress-responsive genes [23]. Deletion of *CUF1* renders *Cn* less virulent in an intravenous
99 mouse model of *cryptococcosis* [32], further underscoring the importance of Cu homeostasis in *Cn*
100 pathogenesis and suggesting the potential of *Cn*Cuf1 as a fungal-specific intervention target to disrupt
101 pathogen-driven adaptations to the host nutritional environment during infection. However, the actual
102 mechanism of high and low Cu gene regulation by Cuf1 in response to various Cu stresses is not well
103 understood and has yet to be elucidated.

104 *Cn*Cuf1 was named and identified based on sequence homologies with the Cu-responsive TF found in
105 *Schizosaccharomyces pombe* (*Sp*), with which it shares the highest sequence homology [32, 33].
106 However, unlike *Sp*Cuf1, which only localizes to the nucleus to direct gene expression of its target genes
107 during Cu limitation, *Cn*Cuf1 is bound to and directs expression of different subsets of target genes
108 during either low or high Cu stress [23, 34]. Despite *Cn*Cuf1's distinct function as dual Cu-responsive TF,
109 it shares conserved, known functional relevant motifs with the previously studied ascomycete Cu-
110 responsive TFs. To further define the molecular mechanisms driving the unique dual activity of this Cu-
111 responsive TF, we mutated these potential functional protein motifs in *Cn*Cuf1 and tested the effects of
112 these mutations on fungal physiology and stress responses. We also explored the consequences of
113 *Cn*Cuf1 mutations targeting the *Cn*Cuf1 high Cu stress response for pathogenesis-relevant cupro-enzyme

114 activity and its effects on pathogenesis within the mouse lung environment using an inhalational mouse
115 model of *cryptococcosis*.

116

117 **RESULTS**

118 **Mutation of the Ace1-like Cys-rich motif in the Cuf1 transcription factor renders the fungus**
119 **susceptible to high Cu stress.**

120 *Cn*Cuf1 is the central Cu-responsive transcription factor known to regulate high and low Cu genes in
121 *Cn* (Fig 1). Sequence comparison between *Cn*Cuf1 and other fungal Cu-responsive transcription factors
122 identified the highest homology within the first 39 amino acids (aa) of the N-terminal domain [23]. This
123 region includes a Zn-binding motif and the highly conserved, positively charged 'KGRP' motif [29, 31, 35-
124 38]. Previous mutational studies in *Cn*Cuf1 have already demonstrated that the KGRP motif is required
125 for promoter binding of both high and low Cu-regulated genes [23] (Fig 1).

126 Following the *Cn*Cuf1 DNA-binding domain, the sequence similarity decreases considerably, except
127 for three cysteine (Cys)-rich motifs, which were previously demonstrated in ascomycete high and low
128 Cu-responsive TFs to be essential for regulation of transcriptional activity; Cu binding to these Cys-rich
129 motifs acts as an ON-OFF switch either activating (Ace1-like transcription factors) or deactivating (Mac1-
130 like transcription factors and *Sp*Cuf1) transcriptional activity [29, 34-36, 39] (Fig 1). The first Cys-rich
131 motif encoded by *CUF1* is formed by an 11 aa motif, containing 4 cysteines, which are highly conserved
132 among Cuf1- and Ace1-like transcription factors [23] (Fig 1B). To elucidate the function of the Ace1-like
133 Cys-rich motif on *Cn*Cuf1 transcriptional activity, we mutated all 4 conserved Cys located in the Ace1-like
134 Cys rich motif to alanine (Ala, Cuf1-FLAG ΔAce1, Supp. Fig 1A). The 2nd and 3rd Cys-rich motif encoded by
135 *CUF1* are formed by a 12 aa motif containing 5 Cys (2nd Cys-rich motif) and a 10 aa motif containing 4
136 cysteines (3rd Cys-rich motif), which are highly conserved among Cuf1- and Mac1-like transcription

137 factors [23] (Fig 1B). Additionally, we identified a sequence of 7 cysteines adjacent to the Mac1-like 3rd
138 Cys-rich motif, which are unique to *Cn*Cuf1 (Fig 1B). To elucidate the function of the Mac1-like Cys-rich
139 motif on *Cn*Cuf1 transcriptional activity, we mutated all 9 conserved cysteines located in the two Mac-
140 like Cys rich motifs encoded by *Cn*Cuf1, as well as the 7 adjacent cysteine residues to alanine (Cuf1-FLAG
141 ΔMac1, Supp. Fig 1A). Alleles encoding FLAG-tagged versions of the Cuf1 wild type (WT) protein, the
142 KGRP-mutant protein, the Cuf1 ΔAce1 mutant and the Cuf1 ΔMac1 mutant proteins were incorporated
143 into the *cuf1Δ* mutant strain at the safe haven 1 site [40], all expressed by the *CUF1* promoter.

144 To explore the effects of the introduced mutations on Cuf1-FLAG protein levels at high and low Cu
145 stress, we conditioned the *CUF1*-FLAG- expressing strains for 3 h in either SC medium + 1 mM $CuSO_4$ (=
146 high Cu stress condition) or SC medium + 1 mM of the extracellular Cu chelator bathocuproinedisulfonic
147 acid (BCS,= low Cu stress condition) at 30°C. Western blot analysis using an anti-FLAG-HRP conjugate
148 demonstrated no differences in Cuf1-FLAG protein levels in response to high or low Cu stress between
149 the WT and any of the Cuf1 mutant proteins, indicating that the introduced site mutations do not affect
150 Cuf1 protein levels (Fig 2A).

151 To determine the physiological effect of the introduced site mutations on regulation of Cu
152 homeostasis during Cu stress, we assessed the ability of each allele to complement the *cuf1Δ* growth
153 phenotypes in high and low Cu stress environments. In all stress conditions, the *CUF1-FLAG* WT allele
154 fully restored growth of the *cuf1Δ* mutant strain, demonstrating that the FLAG-tag did not compromise
155 Cuf1 protein function (Fig 2B). In contrast, the KGRP-mutant protein, which was previously
156 demonstrated to lack *Cn*Cuf1-promoter binding capability, predictably did not complement the growth
157 phenotypes of a *cuf1Δ* mutant strain [23]. Consistent with the postulated function of the Ace1-like Cys-
158 rich motif for regulating high Cu stress responses, a *CUF1-FLAG* ΔAce1 mutant allele failed to
159 complement the *cuf1Δ* growth defect in a high Cu environment, however it fully complemented the
160 *cuf1*Δ low Cu growth phenotype (Fig 2B). This finding suggests a specific role for the Ace1- like Cys rich

161 motif for regulating transcriptional activity in response to high Cu stress. In contrast to the assumed
162 function of the two identified Mac1-like Cys-rich motifs for low Cu stress sensing, the Cuf1-Flag ΔMac1
163 mutant allele fully complemented the *cuf1*Δ growth defects in presence of both high and low Cu stress.
164 This finding suggests that *Cn*Cuf1 senses and regulates low Cu stress independent from the Mac1-like
165 Cys-rich motifs (Fig 2B).

166 **The *Cn*Cuf1 C-terminal unstructured domain is required for regulating *Cn*Cuf1transcriptional**
167 **activity**

168 In addition to the N-terminally located conserved DNA binding domain and the Cys-rich motifs,
169 Cn*CUF1* encodes a C-terminal unstructured domain of unknown function, which is unique to *Cn*Cuf1 and
170 not found in any of the studied ascomycete Cu-responsive TFs [23]. The biological function of this
171 extended unstructured C-terminus, and its role for Cu-dependent regulation of *Cn*Cuf1 activity, are
172 unknown. To better understand and define regions required for high and low Cu stress adaptation, we
173 performed a sequential C-terminal truncation analysis of the *Cn*Cuf1 transcription factor using the *CUF1-*
174 *FLAG* WT allele-encoding plasmid (Supp. Fig 1B). Alleles encoding the FLAG-tagged versions of the
175 generated *CUF1-FLAG* truncations were incorporated into the *cuf1Δ* mutant strain at the safe haven 1
176 genomic site [40], all expressed by the *CUF1* promoter.

177 To explore the effects of the introduced truncations on Cuf1-FLAG protein levels at high and low Cu
178 stress, we conditioned the *CUF1-FLAG* truncation-expressing strains as described above and performed
179 western blot analysis using an anti-FLAG-HRP conjugate. All generated *CUF1-FLAG* truncations were
180 expressed at similar protein levels independent from the Cu stress condition (Fig 2C).

181 Like the generated *CUF1* Cys-site mutant strains, we assessed the ability of each *CUF1-FLAG* fragment
182 to complement the *cuf1Δ* growth phenotype in high and low Cu stress environments. Surprisingly, none
183 of the generated *CUF1-FLAG* fragments fully complemented the *cuf1Δ* mutant phenotypes in either Cu

184 stress condition (Fig 2D). Only the largest generated *CUF1-FLAG* fragment (Δ780), which still encodes for
185 a portion of the unstructured C-terminus unique to *Cn*Cuf1, showed a partial growth restoration of the
186 *cuf1Δ* high Cu stress growth defect (Fig 2D, 0.1mM $CuSO_4$). This finding suggests an important role of the
187 unique C-terminal region for regulation of *Cn*Cuf1 transcriptional activity.

188 **The Ace1-like Cys-rich motif is required for Cuf1 to specifically regulate high Cu-responsive genes**

189 To correlate the observed growth phenotypes of the *CUF1-FLAG* Cys-rich motif mutant strains with
190 *Cn*Cuf1 transcriptional activity, we used a dual fluorescent Cu sensor strain to simultaneously measure
191 the activation of the low Cu-regulated *CTR4* gene, encoding for a high affinity Cu importer, as well as the
192 high Cu-regulated *CMT1* gene, encoding for a Cu detoxifying metallothionein. To create the Cu sensor
193 strain, a *CTR4* promoter (p*CTR4*)-driven *mCLOVER* gene and an *CMT1* promoter (p*CMT1*)-driven *mRUBY*
194 gene were inserted into the safe haven 2 site of the *Cn* genome, a "neutral" genomic locus into which
195 new allele introduction does not result in alterations of physiology or virulence [41](Supp. Fig 2A). Doing
196 so resulted in a strain expressing green fluorescence during Cu limitation (induction of p*CTR4* driven
197 *mCLOVER* expression) and expressing red fluorescence during excess Cu (induction of p*CMT1*-driven
198 *mRUBY* expression, Supp. Fig 2B-C). To measure the effects of the *CnCUF1* Cys-rich motif mutant alleles
199 on *Cn*Cuf1 transcriptional activity, we introduced the green- and red-fluorescent Cu sensor alleles into
200 the WT and the *cuf1*Δ mutant; as well as the *cuf1*Δ mutant strain expressing either the *CUF1-FLAG WT*
201 allele, *CUF1-FLAG KGRP-AAAA* mutant allele or the *CUF1-FLAG* Cys-rich motif mutant alleles. All strains
202 were cultured for 24 h in SC medium supplemented with either 50 µM $CuSO_4$ (=excess Cu) or 50 µM BCS
203 (=low Cu) at 30°C prior to protein extraction and western blot analysis of mClover and mRuby protein
204 levels (Fig 3A).

205 Consistent with previously published transcript analysis of Cu- and Cuf1-dependent genes [23], the
206 WT Cu-sensor strain showed robust activation of p*CTR4*-driven *mCLOVER* expression when grown in Cu-

207 limiting conditions (SC+ 50 µM BCS) and robust activation of p*CMT1*-driven *mRUBY* expression during Cu
208 excess (SC +50 µM $CuSO_4$). As predicted by the established activity of *Cn*Cuf1 to control the expression
209 of low and high Cu-responsive genes, deletion of the *CUF1* gene resulted in a failure of Cu-dependent
210 gene activation as measured by the absence of mClover and mRuby protein expression (Fig 3A).
211 Introduction of the *CUF1-FLAG* WT allele, which fully complemented the Cu-stress growth defects of the
212 *cuf1Δ* mutant strain, also fully restored the Cu-dependent mClover and mRuby protein levels to WT-like
213 levels. In contrast, expression of the *CUF1-FLAG* KGRP-AAAA DNA binding mutant, which failed to
214 complement the *cuf1Δ* mutant growth phenotypes, showed similarly absent *mCLOVER* and *mRUBY*
215 expression as the *cuf1Δ* mutant strain.

216 In line with their ability to complement the *cuf1Δ* low Cu stress growth phenotype, neither Cys-
217 rich motif mutations (ΔAce1 or ΔMac1) affected *mCLOVER* expression levels during Cu limitation (Fig
218 3A). However, a slightly higher m*CLOVER* expression was observed for the *CUF1*-FLAG ΔMac1 strain
219 when grown in Cu excess, suggesting a potential role for the Mac1-like Cys-rich motifs to facilitate
220 complete repression of low Cu-regulated genes, such as *CTR4*, when Cu is in excess. No effect on *mRUBY*
221 expression was observed in the *CUF1*-FLAG ΔMac1 expressing strain at either Cu conditions, suggesting
222 that these Mac1-like regions are not involved in the activation of genes induced in high Cu
223 environments. In contrast, mutation of the Ace1-like Cys-rich motif fully inhibited the high Cu-driven
224 activation of *mRUBY* expression. Hence, the previously observed growth defect of the *CUF1*-FLAG ΔAce1
225 expressing strain in presence of high Cu stress is likely due to failed activation of genes required for Cu
226 detoxification. Together, the Cu sensor expression data as well as the Cu stress growth data suggests
227 that mutation of the Ace1-like Cys- rich motif results in an uncoupling of *Cn*Cuf1-directed high Cu and
228 low Cu stress adaptation, with the high Cu stress adaptation being completely blunted while the low Cu
229 stress adaptation seems to be fully functional.

230 To further validate the observed gene expression phenotype of the *CUF1-FLAG*-ΔAce1 mutant strain,
231 we directly measured transcript levels for established high and low Cu-regulated genes using
232 quantitative reverse transcriptase PCR (qRT-PCR) in the WT strain, the *cuf1*Δ mutant strain, as well as
233 the *cuf1*Δ mutant strain expressing either the *CUF1-FLAG WT* allele or the *CUF1-FLAG* ΔAce1 allele. As a
234 measure of high Cu stress transcriptional responses, we measured transcript abundance of the *CMT1*
235 gene, whose promoter was used in the Cu sensor strain, and the *ATM1* gene, encoding for a
236 mitochondrial inner membrane ABC transporter involved in cytosolic Fe-S assembly [21, 24]. To assess
237 responses to low Cu stress, we measured the transcript abundance of the *CTR4* gene, whose promoter
238 was used in the Cu sensor strain, and the *CBI1* gene, encoding the copper binding and release protein 1
239 [22, 23, 28].

240 The above indicated strains were incubated for 3 h in SC medium supplemented with either 1 mM
241 $CuSO_4$ (=high Cu stress condition) or 1 mM BCS (=low Cu stress condition) at 30°C prior to RNA
242 extraction. Transcript levels of the Cu-response genes for each strain in each condition were determined
243 by qRT-PCR. Consistent with prior results, the expression of the *CMT1* and *ATM1* genes was induced in
244 the WT strain under high Cu conditions, and the *CTR4* and *CBI1* genes were induced in low Cu conditions
245 (Fig 3B-C) [23]. In contrast, the transcript levels of both high Cu and low Cu genes were not induced in
246 either condition in the *cuf1*Δ mutant. The *CUF1-FLAG* WT strain fully restored WT levels of Cu-regulated
247 gene expression in both conditions. However, consistent with the observed Cu stress growth
248 phenotypes and the observed mClover and mRuby protein expression profile, mutation of the Ace1-like
249 Cys-rich motif was associated with defective transcriptional activation of high Cu-regulated genes (*CMT1*
250 and *ATM1*, Fig 3C), while fully restoring WT transcript levels of genes involved in low Cu stress response
251 (*CTR4* and *CBI1*) (Fig 3B).

252

253 **The Ace1-like Cys-rich motif is required for Cuf1 binding to high Cu-responsive gene promoters**

254 The Cuf1 transcription factor was previously demonstrated to directly bind the promoters of
255 these high- and low-Cu reporter genes [23]. We used chromatin immunoprecipitation followed by
256 quantitative PCR analysis (ChIP-PCR) to determine whether the observed differential transcript levels in
257 each strain were associated with changes in Cuf1 promoter binding. We specifically chose
258 oligonucleotides corresponding to the *CTR4* and *CMT1* promoters as indicators of low- and high-Cu
259 stress gene promoter binding, respectively. To do so, we incubated the strains in the identical high- and
260 low-Cu stress conditions as above prior to protein-DNA crosslinking and chromatin
261 immunoprecipitation. Enrichment of the *CMT1* or *CTR4* promoter fragments in each sample was
262 calculated relative to the WT strain and was further normalized against the *TUB1* tubulin gene as a non-
263 Cuf1 target gene. Consistent with previous studies, we observed a significant enrichment of the *CMT1*
264 promoter, but not the *CTR4* promoter, in the Cuf1-FLAG WT sample conditioned in high Cu stress, and
265 enrichment of the *CTR4* promoter sequence during low Cu stress [23](Fig 3D-E). In contrast, no
266 enrichment of the *CMT1* promoter was observed by ChIP-PCR in the *cuf1*Δ + *CUF1-FLAG* ΔAce1 strain
267 conditioned in high Cu stress, whereas the *CTR4* promoter was enriched in this strain to similar levels as
268 in the Cuf1-FLAG WT allele expressing strain (Fig 3D-E). Taken together, these data demonstrated that
269 the Ace1-like Cys-rich motif is required for Cuf1 binding to and regulation of high Cu-responsive
270 promoters while it does not impact binding or regulation of low Cu-responsive promoters.

271 Together, these transcript and promoter binding data demonstrate that the Ace1-like Cys-rich motif
272 is required for the *Cn*Cuf1 transcription factor to transcriptionally activate high Cu-responsive genes but
273 not low Cu-responsive genes. This activity likely explains the defective cellular adaptation to high Cu
274 stress for strains with mutations of this site.

275

276 **The Ace1-like Cys-rich motif is required for proper regulation of ROS detoxification and melanization**
277 **in high Cu environments.**

278 *Cn* encounters both low- and high-Cu microenvironments in the infected host [22]. A full loss-of-
279 function mutation of the *CUF1* gene ultimately affects both high and low Cu stress adaptation, which
280 complicates the analysis of high Cu or low Cu stress responses for *Cn* pathogenesis. Our mutational
281 analysis identified the *CUF1-FLAG*-ΔAce1 mutant strain as a candidate strain to specifically analyze the
282 role of high Cu stress adaptation for *Cn* pathogenesis. First, we assessed the role of Cuf1 and the Ace1-
283 like Cys-rich motif for the activity of cupro-enzymes required for *Cn* stress resistance and survival within
284 specific microenvironments of the human host.

285 <u>Laccase 1 and melanin production:</u>

286 The *Cn*Lac1 protein is a Cu-containing diphenol oxidase/laccase involved in formation of
287 melanin, a cell wall-associated pigment that protects the fungus from host-derived oxidative and
288 nitrosative stress as well as from antifungal drugs [42]. The process of melanization is tightly linked to Cu
289 homeostasis and Cuf1 regulation in multiple ways. First, melanin production requires cellular Cu as Lac1
290 oxidase activity is dependent on Cu as a catalytic cofactor [43]. Second, *LAC1* gene expression is
291 controlled in a Cuf1-dependent manner [23, 27, 44, 45](Fig 4A). To analyze the effects of the Ace1-like
292 Cys site mutation on melanin production, we incubated the WT strain, the *cuf1*Δ mutant, and the *cuf1*Δ
293 strain expressing either *CUF1-FLAG* WT or the ΔAce1-like Cys site mutant allele on L-DOPA medium
294 supplemented with either 10 μM BCS (to slightly restrict Cu) or 10 μM $CuSO_4$ (to provide excess Cu). As
295 controls, we included the completely melanin-defective *lac1*Δ mutant strain and the *cbi1*Δ *ctr4*Δ double
296 mutant strain that is impaired in copper import [28, 43]. For each strain, relative *LAC1* transcript levels
297 were measured after 3 h of incubation in liquid L-DOPA medium similarly supplemented with either 10
298 μM BCS or 10 μM $CuSO_4$.

299 The WT strain was strongly melanized by 72 h, and the addition of excess Cu to the medium
300 resulted in a higher degree of pigmentation (Fig 4B). In contrast, the *cuf1*Δ mutant displayed decreased
301 melanin in Cu-limited conditions, similar to that of the *cbi1*Δ *ctr4*Δ Cu import mutant (Fig 4B)[28, 46]. In
302 these conditions, *LAC1* gene expression in the *cuf*1Δ mutant was similar to WT, suggesting that the
303 observed decreased melanin formation in the *cuf1*Δ mutant is due to failed induction of Cu import
304 genes, such as *CTR4*, resulting in reduced levels of intracellular Cu (Fig 4C-D). Consistent with this
305 hypothesis, we observed full restoration of melanization in the Cu-import mutant with Cu
306 supplementation, restoring Lac1 Cu loading and thus enzymatic function (Fig 4B).

307 In contrast to the Cu import mutant, melanin formation was not restored in the *cuf1*Δ mutant
308 when the medium was supplemented with Cu. On the contrary, the *cuf1*Δ strain demonstrated an even
309 more severe melanin-deficient phenotype, similar to that of the *lac1*Δ mutant (Fig 4B). In contrast to
310 intact *LAC1* expression during Cu-limitation, we observed a marked relative decrease in *LAC1* transcript
311 levels in the *cuf1*Δ mutant strain in Cu-excess conditions, consistent with the role of Cuf1 supporting
312 *LAC1* expression when Cu is present in excess. (Fig 4C).

313 Reintroduction of the *CUF1-FLAG* WT allele fully restored WT levels of melanin production in
314 both high and low Cu environments, as well as WT levels of *LAC1* and *CTR4* expression (Fig 4B-D). In
315 contrast, the *cuf1*Δ strain expressing the ΔAce1-like Cys site mutant allele only restored melanization
316 when Cu was limited but not when Cu was present in excess (Fig 4B). In this strain, *CTR4* expression was
317 fully restored in Cu-limiting conditions, but *LAC1* expression was not restored in Cu excess (Fig 4C-D).
318 Taken together, these data demonstrate a major role for Cuf1 in controlling melanin formation, by
319 ensuring adequate levels of Cu as catalytical cofactor for Lac1 in low Cu conditions, and by supporting
320 *LAC1* gene expression in higher Cu conditions. Additionally, the Cuf1 Ace1-like Cys-rich motif is required

321 for ensuring proper *LAC1* expression and melanization when Cu is present in excess but is not required
322 for melanization during Cu limitation.

323 The effect of *Cn*Cuf1 on superoxide dismutase (SOD) expression and ROS detoxification

324 The Cu, Zn-superoxide dismutase Sod1 helps to protect the fungal cell from ROS generated by
325 host immune cells during infection [26]. Previous studies demonstrated that Cuf1 binds to the *SOD1*
326 promoter and induces *SOD1* gene expression in high Cu stress. In contrast, during prolonged Cu
327 starvation, *SOD1* expression is repressed to divert limited Cu from this Cu-containing enzyme to support
328 other Cu-dependent cell processes. In this condition, Cuf1 binds to the *SOD2* promoter and induces the
329 expression of a cytosolic retained variant of this Mn-dependent mitochondrial superoxide dismutase to
330 uncouple ROS detoxification from a Cu-requiring enzyme when cellular Cu is scarce [11]. Therefore,
331 deletion of *CUF1* renders cells vulnerable to ROS stress not only during high Cu stress due to failure of
332 up-regulation of *SOD1* but also during low Cu stress due to inability to switch to a Cu-independent ROS
333 detoxification pathway (Fig 5A).

334 To test the effects of the Ace1-like Cys-rich motif mutation on cellular ROS detoxification, we
335 incubated the WT and *cuf1*Δ strains, as well as strains expressing *CUF1-FLAG* WT or the ΔAce1-like Cys
336 mutant allele, in the presence of increasing concentrations of the superoxide-generating compound
337 menadione by disc diffusion (Fig 5B). Consistent with previous studies, the *cuf1*Δ mutant showed an
338 increased susceptibility to menadione, measured by zone size of growth inhibition, in both high and low
339 Cu conditions (Fig 5C) [11]. Both Cu-stress phenotypes were fully restored in the *cuf1*Δ strain expressing
340 the *CUF1-FLAG* WT allele. In contrast, the strain expressing the *CUF1-FLAG* ΔAce1-like Cys mutant allele
341 only restored ROS resistance during low Cu stress but not high Cu stress (Fig 5C).

342 To fully analyze the role of the Ace1-like Cys motif in regulating SOD-driven ROS detoxification,
343 we measured Sod activity in whole cell extracts using an in-gel Sod activity assay [10] from cells

344 conditioned in either low or high Cu stress. The Sod activity gels demonstrated three activity bands from
345 cell extracts from the WT strain incubated in low Cu conditions. The lowest band likely represents Sod1,
346 while the middle band likely represents Sod2 activity given their absence in the respective *sod1*Δ and
347 *sod2*Δ mutants (Fig 5D). The highest of the three bands was absent in the *cuf1*Δ and *sod2*Δ mutant
348 strains (Fig 5D, yellow hash tag), and likely represents the cytosolic Sod2 variant that is specifically
349 enriched in Cu limitation in a Cuf1-dependent manner [11]. This Sod activity is restored in the *cuf1*Δ
350 mutant by introduction of either the *CUF1-FLAG* WT or the ΔAce1-like Cys site mutant allele, indicating
351 that Cuf1-dependent formation of cytosolic Sod2 during Cu-limiting conditions is not dependent on the
352 Cuf1 Ace1-like Cys motif (Fig 5C-D).

353 The patterns of SOD activity varied when the strains were conditioned in high Cu stress, with
354 two predominant bands of similar intensity in WT cells. Both bands were significantly reduced in
355 intensity in the *cuf1*Δ mutant strain. Moreover, in the *sod1*Δ strain, these two bands were only faintly
356 present, and the upper of these two was either not present or altered in its molecular size (Fig 5D,
357 yellow asterix), suggesting that this upper band represents Sod1 activity. While expression of *CUF1-FLAG*
358 WT restored the Sod activity bands to WT-like levels, we observed identical patterns of reduced Sod
359 activity in the *cuf1*Δ mutant as well as the *cuf1*Δ mutant expressing the *CUF1-FLAG* ΔAce1-Cys mutant
360 allele, indicating that the first Cys-rich motif is required for Cuf1-depenedent induction of Sod1 protein
361 activity in response to high Cu stress (Fig 5D). Consistent with this finding, the Cuf1 Ace1-like Cys-rich
362 motif is required for supporting Cuf1-dependent *SOD1* transcript induction in high Cu conditions (Fig 5E).
363 Together, these phenotypic data, enzyme activity assays, and transcript assessments demonstrate the
364 importance of the Ace1-like Cys-rich motif for Cuf1-dependent regulation of ROS detoxification in a high
365 Cu stress environment.

366

367 **Consequences of a blunted Cuf1 high Cu stress response on fitness, yeast containment and immune**
368 **response inside the host lung environment**

369 A previous study conducted by Waterman *et al.* established a role for Cuf1 for virulence in an
370 intravenous model of *Cn* infection, demonstrating a decreased fungal burden of the *cuf1*Δ mutant
371 compared to WT in the mouse brain but not in the mouse lung [32]. More recent studies have suggested
372 that these different anatomic sites represent different Cu environments encountered by *Cn* during the
373 course of infection [21, 22, 28]. Using high and low Cu promoter-driven Luciferase strains, one study
374 demonstrated an up-regulation of genes typically induced during Cu deficiency in the brain, while the
375 lung environment induced genes required for Cu detoxification [21]. This finding was further
376 underscored by assessment of the effects of Cu homeostasis mutant strains on virulence and survival at
377 the different sites of infection: strains lacking components of the Cu import machinery were less fit
378 within the mouse brain environment, while strains lacking components required for Cu detoxification
379 were less fit in the mouse lung environment [21, 22, 28].

380 Given the high Cu stress phenotypes observed *in vitro* for the *cuf1*Δ mutant and the ΔAce1-like
381 Cys-rich motif mutant strain, we hypothesized that these strains would display altered physiology within
382 the high Cu environment of the lung. We inoculated female A/J mice by inhalation with the WT strain,
383 the *cuf1*Δ mutant, or the *cuf1*Δ mutant reconstituted with either the WT *CUF1-FLAG* allele or the *CUF1-*
384 *FLAG* ΔAce1 mutant allele. Lungs were harvested at 14 days post infection, a time point at which lung
385 infection is well established but before animals succumb to infection. In the infected lungs, we assessed
386 lung fungal burden as well as relative patterns of inflammation by histology and flow cytometry analysis
387 (Fig 6, Supp. Fig 3). Consistent with prior studies, we did not observe significant difference in lung fungal
388 burden for any of the analyzed strains at this infection time point (Fig 6A) [32]. However, we did note a
389 significant increase in lung wet weight in animals infected with the WT or *CUF1-FLAG* WT strain

390 compared to the lungs of mice infected with the two high Cu response-defective strains (Fig 6B).
391 Additionally, we observed macroscopic differences between WT and *CUF1-FLAG* WT-infected lungs
392 compared to *cuf1*Δ- and the *CUF1-FLAG* ΔAce1-like Cys-rich motif mutant-infected lungs: WT-infected
393 lungs demonstrated more extensive foci of tissue abnormality (darkening) compared to lungs infected
394 with either the *cuf1*Δ mutant or the ΔAce1-like Cys-rich motif mutant strain (Fig 6C, white arrows).

395 Histopathology analysis of fixed lung tissue demonstrated similarly altered patterns of
396 inflammation and yeast containment between these two groups. The regions of lung tissues
397 characterized by intense inflammation were demarcated and quantified relative to the total lung area.
398 These measures demonstrated significantly more regionally extensive lung inflammation in mice
399 infected with the WT strain or the *CUF1-FLAG* WT strain compared to either the *cuf1*Δ mutant or the
400 Ace1-like *cuf1*Δ mutant strains (Fig 6D-E, yellow highlighted areas). While lungs infected with the WT
401 strain displayed expected patterns of diffuse inflammation surrounding single and grouped
402 encapsulated yeast cells throughout the lung tissue (Fig 6F) [47], the *cuf1*Δ mutant strain displayed yeast
403 cells mostly confined to well circumscribed foci, similar to the early granulomas described previously in
404 studies of *Cn* strains with slow growth phenotypes due to defects in mitochondrial function [47]. Also
405 compared to WT, the *cuf1*Δ mutant-infected lungs displayed a very sharp distinction between inflamed
406 regions containing encapsulated yeast cells and normal-appearing lung tissue with no apparent yeast
407 cells present (Fig 6F).

408 Lungs infected with the *CUF1-FLAG* WT-expressing strain demonstrated similar patterns of
409 inflammation as observed in WT-infected lungs (Fig 6D-F). In contrast, the *CUF1-FLAG* ΔAce1-like Cys-
410 rich motif mutant expressing strain generated an infection pattern similar to *cuf1*Δ-infected lungs, with
411 smaller and more contained areas of inflammatory cells intermixed with yeast cells surrounded by
412 normal-appearing lung tissue with no apparent yeast cells (Fig 6D-F). These findings suggest that Cuf1-

413 regulated high Cu responses are not required for absolute fitness within the mouse lung environment
414 but instead modulate colonization patterns, yeast containment, and inflammation at the site of
415 infection.

416 We also performed flow cytometry to test whether the different lung infection patterns
417 observed histologically in WT- versus *cuf1Δ* mutant-infected lungs were marked by changes in the
418 immune cell populations. Despite the observed macroscopic and microscopic differences between the
419 WT- and mutant-infected lungs, we noted no significant differences at this 14-day infection time point in
420 the relative percentages of immune cell subtypes (Total Myeloid cells - Neutrophils, Monocytes,
421 Eosinophils, and Dendritic cells as well as Total Lymphocytes - B cells and T cells) or T cell activation
422 markers (IFN γ, IL-17A and IL-4 measured in $CD4^+$, $CD8^+$ and γΔ T cells, Supp. Fig 3).

423

424 Discussion

425 *Cn*Cuf1 is unique among fungal Cu-responsive transcription factors as it regulates a diverse
426 spectrum of Cu responses, combining the role of a high Cu-responsive transcription factor with the role
427 of a low Cu-responsive transcription factor [23]. Accordingly, it shares conserved motifs with both high
428 and low Cu-responsive transcription factors previously identified in model ascomycete yeast Cu
429 transcription factors [23]. Previous research in these ascomycete model yeasts has demonstrated that
430 Cu binds directly to these Cys-rich motifs and thus modulates protein confirmation. These
431 confirmational changes result in either activation (Ace1-like high Cu-responsive TFs) or inhibition of Cu-
432 responsive transcriptional activity (Mac1-like low Cu-responsive TFs) [35, 36, 38, 39, 48].

433 While these regulatory Cys-rich motifs are conserved in fungal Cu-responsive TFs, their precise
434 molecular function for regulation of Cu-responsive transcriptional activity has evolved differently in
435 different fungal clades. For instance, an interspecies cross-complementation study conducted with the

436 *Aspergillus fumigatus* (*Af*) AceA high Cu-responsive transcription factor demonstrated that AceA
437 homologs from ascomycete yeasts did not functionally complement the high Cu growth defect observed
438 in the *Af* Δ*aceA* mutant, suggesting that, even though the N-terminal DNA binding and the Cu sensing
439 motifs are highly conserved among these high Cu-responsive transcription factors, the motifs might
440 function differently in *Aspergillus* species than in their yeast counterparts [49]. Another example for this
441 divergence is the Cu-responsive TF, *Sp*Cuf1, found in fission yeast, which encodes for an Ace1-like Cys-
442 rich motif and an additional Mac1-like Cys-rich motif. Here, Cu binding to its Cys-rich motifs does not
443 only result in transcriptional inhibition but also cytosolic re-localization of the TF when Cu is in excess
444 [33, 34, 50]. Among the characterized fungal Cu-responsive TFs *Cn*Cuf1 demonstrates the largest
445 divergence, having evolved into a dual Cu-stress responsive transcription factor, which directly binds to
446 and regulates different subsets of target genes in response to low and high Cu stress. *Cn*Cuf1 is not only
447 the first described dual Cu-responsive TF, but it also regulates Cu stress adaptation of a basidiomycete
448 fungus, which is distantly related to the well-studied model ascomycetes. Our research reinforces this
449 evolutionary divergence; while the Ace1-like conserved Cys-rich motif maintained its functional
450 relevance for *Cn*Cuf1 high Cu stress adaptation, the Mac1-like Cys-rich motifs lost their predominant role
451 in regulating low Cu stress adaptation. Furthermore, the absolute dependence on the presence of the
452 unstructured *Cn*Cuf1 C-terminal domain for Cu stress sensing and adaptation further underscores the
453 evolutionary reshaping of molecular mechanisms driving *Cn*Cuf1 transcriptional activity. Additional
454 research will be necessary to fully understand the molecular mechanisms behind the *Cn*Cuf1 Cu-
455 dependent transcriptional activity, and further phylogenetic studies will be required to define the
456 diversity of Cu stress sensing within the fungal kingdom.

457 The transition metal Cu has been established as an important virulence factor in all major
458 human fungal pathogens as it is used as a cofactor for several enzymes required for stress adaptation
459 within the host [10, 11, 42, 51, 52]. Accordingly, Cu import genes and the Cu-responsive transcription

460 factors sensing and maintaining the cellular Cu quota have been demonstrated to play an important role
461 in fungal pathogenesis [12, 22, 28, 32, 53-55]. For instance, in *Candida albicans* (*Ca*) researchers
462 demonstrated that the low Cu-responsive *Ca*Mac1 transcription factor is required for host invasion,
463 adhesion to host cells, and antifungal tolerance [53]. Similarly, mutation of the low Cu-responsive MacA
464 transcription factor in *Af* attenuates pathogenicity in a neutropenic immunocompromised mice model
465 [54].

466 Nutritional immunity responses for other transition metals mostly involve sequestering these
467 micronutrients from the sites of infection [15, 17]. In contrast, Cu nutritional immunity responses appear
468 to be more dynamically regulated and are highly tissue dependent. While Cu might be restricted at one
469 site or time point of an infection, elevated and toxic Cu levels are present at other sites or time points to
470 act as an antimicrobial agent to kill the invading pathogen [10-13, 16, 21, 22, 56]. Therefore, high Cu
471 stress responses are as important as Cu scavenging responses for microbial pathogenesis. However,
472 both responses must be balanced to ensure proper adaptation to the Cu environment established at the
473 particular infection micro-niche.

474 Analysis of the dynamic shifts in the host and microbial physiology associated with Cu nutritional
475 immunity responses has been challenging to study in *Cn* since deletion of the *CUF1* gene ultimately
476 blunts both high and low Cu stress responses [23]. This makes deciphering the role of high and low Cu
477 stress responses during infection difficult as these stresses can have compensatory effects. For instance,
478 deletion of the *CTR4* Cu importer gene was shown to be beneficial for *Cn* survival during pulmonary
479 infection, preventing an excessive influx of Cu and thus reducing the toxic effect of the high Cu lung
480 environment. In contrast, the same gene deletion resulted in reduced fungal virulence when the strain
481 was directly injected into the CNS, a site where Cu is limited [22]. Our mutational study aimed to identify
482 amino acid motifs specifically required for transcriptional activity in high or low Cu environments to
483 uncoupled *Cn*Cuf1-driven high Cu stress responses from low Cu stress responses. In this work using a

484 combination of transcriptional analysis, Cu stress phenotypic analysis, and enzyme activity assays, we
485 established an essential role for the Ace1-like Cys-rich motif for *Cn*Cuf1 transcriptional activity during
486 high Cu stress. Importantly, mutation of this site does not affect low Cu stress adaptation. Using this site
487 mutant, we were able to demonstrate the consequences of a blunted high Cu stress adaptation on Cu-
488 dependent virulence factor expression *in vitro* and on fungal growth, dissemination and inflammation *in*
489 *vivo.*

490 Recent work conducted with *Af*AceA demonstrated that mutation of its conserved Cys-rich
491 region attenuates virulence of the fungus similar to a complete Δ*aceA* mutation [49], highlighting the
492 importance of this Cys-rich motif for activating Cu stress responses within the mouse lung environment.
493 Similar to a Δ*aceA* mutant in *Af*, deletion of the *CnCUF1* gene results in an attenuation of virulence [32].
494 However, unlike the *Af* Δ*aceA*, a *CUF1* deletion did not affect *Cn* growth inside the lung environment [32,
495 49]. This observation stands in contrast with the severe *in vitro* phenotypes exhibited by the *cuf1Δ*
496 mutant and the *CUF1-FLAG* ΔAce1 motif mutant strains during high Cu stress. The observed *in vivo*
497 growth phenotype of the *cuf1Δ* and the *CUF1-FLAG* ΔAce1 mutant is also very different from the
498 strongly attenuated phenotype observed for a *Af* Δ*aceA* mutant. These very distinct outcomes of a
499 blunted high Cu stress response observed in the pathogenesis of two fungal pathogens in the same host
500 organ suggest different host-pathogen dynamics within the lung Cu environment, which are likely
501 dependent on the type of pathogen and its lifestyle inside the host tissue. For example, the hyphal
502 fungus *Af* exists primarily extracellularly in the infected lungs, whereas the yeast-like *Cn* survives both
503 intracellularly within host immune cells and extracellularly in the lung tissue. Another possibility is that
504 *Cn* might not be as dependent on Cuf1 as *Af* on AceA for Cu detoxification *in vivo*. For instance, *Cn* could
505 have evolved alternate compensatory mechanisms to survive in the host lung environment which are
506 independent from Cuf1. To address these questions and to better understand the dynamics of Cu

507 nutritional immune responses within the lung environment, a more thorough assessment is needed at
508 several different stages of infection.

509 Although we did not observe significant differences in fungal burden between our WT and
510 mutant strains at two weeks of infection, we did observe macroscopic and microscopic differences
511 within the lungs of WT-infected mice compared to mice infected with the *cuf1*Δ mutant or *CUF1-FLAG*
512 ΔAce1 site mutant. This observation suggests a role for *Cn*Cuf1-driven high Cu stress responses for
513 modulating inflammatory responses within the lung environment, by potentially mediating adaptive
514 responses at the fungal cell surface. This fungal feature is composed of ordered layers of
515 polysaccharides and mannosylated proteins and is the site of recognition and interaction with the host
516 immune system. Changes in carbohydrate composition, as well as masking or unmasking of certain cell
517 surface components, can modulate and define the pattern of inflammation caused by the pathogen [57-
518 59]. For instance, chitin has been associated with non-protective immune responses, and the degree of
519 chitin masking, coupled with the relative amount of chitosan within the *Cn* cell wall, modulates the
520 severity of immune recognition and inflammation within the host tissue [59, 60].

521 Previous work has suggested that the fungal cell wall also plays a role in regulating intracellular
522 Cu levels during Cu stress [27]. In turn, *Cn*Cuf1 regulates multiple genes associated with the fungal cell
523 wall in response to Cu stress [23, 27]. Another study showed that cell wall architecture and cell wall
524 chitosan levels are significantly altered in a *Cn* Cu homeostasis mutant strain during Cu limitation [27].
525 These findings document a role for Cu and *Cn*Cuf1 in modulating the fungal cell wall. Hence, one
526 possible explanation for the observed altered macroscopic and microscopic phenotypes could be that
527 the impaired high Cu stress response in these mutant strains prevented Cu-stress-driven cell wall
528 remodeling and thus modulated immune recognition and yeast dissemination, which could trigger a
529 more focal, granuloma-like inflammatory response with fungal containment within these inflammatory
530 foci. However, we did not observe any significant changes of the relative percentages of immune cell

531 subtypes or T-cell activation, which could explain the altered microscopic features found in mutant-
532 infected lungs.

533 Another possible explanation of the altered yeast distribution observed in mutant-infected lungs
534 could be the presence of different Cu nutritional micro-niches restricting dissemination of yeast cells
535 with an impaired high Cu stress adaptation to lung micro-niches presenting a more favorable, non-toxic
536 Cu environment. This model is supported by previous research demonstrating the mouse lung to be a
537 high Cu environment, which induces *Cn* Cu detoxification genes [21, 22]. However, no clear data is
538 available which lung micro-niches might induce the *Cn* high Cu stress responses. Further investigations
539 will more precisely define the interplay between Cu availability within different host micro-niches, the
540 effects of Cu and *Cn*Cuf1 on the fungal cell surface and their impact on fungal dissemination and
541 immune recognition at different stages and sites of infection.

542

543 Materials and Methods

544

545 Ethics statement

546 All animal experiments conducted in this study were approved by the Duke University
547 Institutional Animal Care and Use Committee (IACUC) (protocol #A102-20-05). Mice were handled
548 according to IACUC guidelines.

549

550 Strains, media and growth conditions

551 *Cryptococcus neoformans* strains used in this study are shown in **Table S1.** Strains generated in
552 this study were created using the *C. neoformans var. grubii H99* background. Strains were created using
553 biolistic transformation or CRISPR/Cas9 method as previously described [61, 62]. Used guide RNA for
554 CRISPR/Cas-based transformations are listed in **Table S2.** Yeast extract (2%)-peptone (1%)-dextrose (2%)
555 (YPD) medium supplemented with 2% agar, 200 µg/ml of hygromycin B (HYG) and 10 µM $CuSO_4$ was
556 used for colony selection after transformation. Transformants were screened by PCR for intended
557 mutations and gene expression was confirmed by western blot. Plasmids and oligonucleotides used in
558 this study for strain generation are listed in **Tables S3-S4.** For strains generated through mating, the
559 corresponding *MAT* a and *MAT* α strain were mixed on to a MS agar and incubated in the dark until
560 basidiospores were formed. Dissected spores were grown on YPD media at 30C for 3-4 days and
561 screened for marker, gene expression (via western blot) and parental Cu-stress phenotypes.
562 Strains were stored and recovered from glycerol stocks (stored at −80°C) and were routinely
563 cultivated in synthetic complete (SC) medium (MP Biomedicals) at 30°C. Media was supplemented with
564 indicated concentrations of $CuSO_4$ or the extracellular Cu^+ chelator bathocuproine disulfonate (BCS) to
565 induce Cu excess, sufficiency or deficiency, respectively.
566 Growth phenotype analysis was performed as previously described [27, 63]. Melanization assays
567 were performed on L-3,4-dihydroxyphenylalanine (L-DOPA) media (7.6 mM L-asparagine monohydrate,
568 5.6 mM glucose, 22 mM KH_2PO_4, 1 mM $MgSO_4$ heptahydrate, 0.5 mM L-DOPA, 0.3 µM thiamine-HCl, 20
569 nM biotin, pH 5.6) as previously described [27, 63]. L-DOPA plates were incubated at 30°C for 3 days.

570 **Trichloroacetic acid (TCA)-based protein precipitation and western blotting**

571 *Cn* cultures were grown overnight for 18 h in synthetic complete (SC) medium (MP Biomedicals)
572 and were Cu-stressed as indicated. TCA-precipitated protein extracts were generated as previously
573 described [64]. Precipitated proteins were solubilized in alkylating buffer (0.1 M Tris pH 8.3, 1 mM EDTA,
574 1% SDS) for 10 min at 65°C. For Cuf1-FLAG western blots, crude TCA extracts were used in all

575 experiments and indicated amounts of the crude TCA extract were treated with 1x SDS-loading buffer
576 (Biorad) and boiled for 10 min at 95°C. For Cu sensor blots, the crude TCA extract was clarified for 10
577 min at 21000 xg and total protein was quantified via BCA assay (Pierce). 20 µg total protein per sample
578 was treated with 1x SDS-loading buffer (Biorad) and boiled for 10 min at 95°C. Protein samples were run
579 on a 7.5% TGX Midi (Cuf1-FLAG) or 4-20 % Midi (Cu Sensor) polyacrylamide gel (Biorad) using SDS
580 running buffer (Biorad) for ~60 min at 150 V. Then, proteins were blotted on nitrocellulose using the
581 Transblot Turbo system (Biorad) at the high molecular weight (Cuf1-FLAG site mutants), mixed
582 molecular weight (Cuf1-FLAG fragment) or standard (Cu sensor) midi blotting setting. Protein transfer
583 was validated via ponceau staining and the membrane was blocked for 1 h at room temperature (RT, for
584 primary antibodies) or overnight at 4°C (for HRP-conjugated antibodies) with 5% Milk in TBS + 0.1%
585 Tween20 (TBS-T). Cuf1-FLAG protein levels were analyzed using a monoclonal Anti-FLAG M2-Peroxidase
586 antibody (1:5000 dilution) (Sigma, α-FLAG-HRP) using a rabbit anti-GAPDH at 1:2000 dilution in 5% milk
587 + TBS-T and 0.02% sodium azide (Abcam, ab9485) combined with an anti-rabbit-HRP in a dilution of
588 1:4000 (GE Healthcare) as loading control. For mClover detection, a mouse anti-GFP at 1:5000 dilution in
589 5% milk + TBS-T and 0.02% sodium azide (Roche, 11814460001) combined with an anti-mouse-HRP in a
590 dilution of 1:4000 (Amersham, NA931V) was used. For mRuby detection, a rabbit anti-RFP at 1:1000
591 dilution in 5% milk + TBS-T and 0.02% sodium azide (Abcam, ab124754) combined with an anti-rabbit-
592 HRP in a dilution of 1:4000 (Amersham, NA934V) was used. As loading control, a rabbit anti-GAPDH
593 antibody was used as described above. Primary antibodies were incubated overnight at 4°C, the FLAG-
594 HRP conjugate as well as secondary antibodies were incubated for 1 h at RT. Blots were blocked with 5%
595 milk in TBS-T and washed 3x for 15 min with TBS-T after each antibody incubation.

596 For detections using multiple primary antibodies, the membrane was stripped using the Restore
597 Western Blot Stripping Buffer (Thermo Fisher Scientific) according to manufacturer's instructions and re-
598 blocked for 30 min in between each primary antibody detection. HRP-conjugated antibodies were

599 detected by chemiluminescence using the DuraWest Pico substrate (Thermo Fisher Scientific).
600 Chemiluminescence was measured using an Azure 600 imager (Azure Biosystems).
601
602 **RNA isolation and quantitative reverse transcriptase (qRT)-PCR**
603 For transcript analysis during high versus low Cu stress, overnight cultures (~18 h) incubated in
604 synthetic complete (SC) medium (MP Biomedicals) were diluted to OD_{600} 0.5, grown for 2 h at 30°C in SC
605 medium. Cu stress was then induced by the addition of either 1 mM BCS or 1 mM $CuSO_4$ and cultures
606 were grown for 3 h at 30°C.
607 For transcript analysis in melanin inducing conditions, overnight cultures grown in SC medium
608 were diluted to OD_{600} 0.5 and incubated for 3 h at 30°C in L-DOPA medium supplemented with either 10
609 µM BCS or 10 µM $CuSO_4$.
610 RNA extraction and cDNA analysis were performed as described previously [27]. For transcript
611 analysis via qRT-PCR, cDNA was diluted 1:5 in RNase-free water and mixed with the PowerUP SYBR
612 Green Master mix (Applied Biosystems) per protocol instruction and analyzed on a QuantStudio 6 Flex
613 (Applied Biosystems). The oligonucleotides used for transcript analysis are listed in **Table S3.** Cycle
614 threshold (C_T) values were calculated using the QuantStudio 6 Flex and gene expression values were
615 normalized to *GAPDH*. Expression fold changes were calculated using the $\Delta\Delta C_T$ method. For all transcript
616 analysis a minimum of 4 independent biological replicates were analyzed.
617
618 **Chromatin immunoprecipitation followed by quantitative PCR (ChIP-PCR) analysis**
619 Overnight cultures (~18 h) grown in SC medium were diluted to OD_{600} 0.2, and incubated for 2 h
620 at 30°C in SC medium. Cu stress was then induced by the addition of either 1 mM BCS or 1mM $CuSO_4$
621 and cultures were grown for 2.5 h at 30°C. Crosslinking of the samples was performed in a 1%
622 formaldehyde solution for 30 min at RT. The downstream processing and ChIP were performed as

623 previously described [23] with the following adaptions: Instead of sonication 5 times, with 30 sec ON
624 followed by 1 min OFF, samples were processed using a Bioruptor UCD200 (Diagenode) via 24 cycles of
625 15 sec "ON " followed by 15 sec "OFF" at the high level to shear chromatin. Immune precipitated DNA
626 fragments were purified with a PCR clean up kit (Macherey Nagel) following manufacturer's instructions.
627 qPCR was performed with the PowerUP SYBR Green Master mix (Applied Biosystems) per protocol
628 instructions and analyzed on a QuantStudio 6 Flex (Applied Biosystems) using oligonucleotides listed in
629 **Table S3**. For quantification, the C_T from each input was subtracted from the C_T from the target gene
630 obtained for the Cuf1–FLAG strain ($\Delta C_{T\ target}$) or the negative control (WT strain, no FLAG-tagged Cuf1,
631 $\Delta C_{T\ control}$). Then, the $\Delta\ C_{T\ control}$ was subtracted from the $\Delta C_{T\ target}$ to give a $\Delta\Delta\ C_T$ value. For each gene
632 promoter, Cuf1 enrichment was calculated as the inverse $\log_2$ of $\Delta\Delta\ C_T$ ($2^{-\Delta\Delta Ct}$). Cuf1-FLAG enrichment at
633 the tubulin promoter was used for normalization.
634
635 **Disc diffusion assay**
636 To measure menadione-induced ROS stress sensitivity, SC overnight cultures (~18 h) of indicated
637 *Cn* strains were diluted 1:500 in SC medium, and 500 µL cell suspension spread onto SC plates or SC
638 plates supplemented with indicated amounts of BCS or $CuSO_4$. Inoculated plates were dried for 45 min
639 at RT. Filter discs were spotted with 15 µL of the indicated concentrations of menadione (dissolved in
640 ethanol) and set in quadrants around the plates. Plates were incubated at 30°C for 3 to 4 days.
641
642 **Protein extraction and Sod activity assay**
643 For Sod activity analysis, *Cn* overnight cultures (~18 h) incubated in SC medium were diluted to OD_{600} 0.1
644 in SC medium or SC medium supplemented with either 250 µM BCS or 50 µM or 100 µM $CuSO_4$. Cultures
645 were incubated for 24 h at 30°C. For protein extraction, cells were pelleted (1 min, 11000 xg, 4°C),
646 washed 1x with cold Lysis buffer (10 mM sodium phosphate, 50 mM NaCl, 0.1% triton X-100, 10%

647 glycerol pH 7.8 made in chelex-treated H_2O) and resuspended in 350 µL of cold lysis buffer + 1x Protease
648 Inhibitor cocktail (ROCHE) and PMSF. Cells were lysed with a Bead Ruptor 12 (Omni international) using
649 6 cycles of 60 sec "ON" and 90 sec "OFF", 5.5 speed at 4°C. Cell lysates were clarified for 15 min at
650 21000 xg at 4°C and the clarified lysate was transferred into a 1.5 mL reaction tube. Total protein levels
651 were measured using a BCA kit (Thermo Fisher Scientific) according to manufacturer's instruction.
652 Lysates were diluted to a concentration of 75 µg protein in 25 µL native sample buffer (Bio-Rad, catalog
653 #1610738) and lysis buffer added to a final volume of 50 µL. Diluted lysates at a volume of 20 µL were
654 loaded onto a 10% mini-PROTEAN TGX precast protein gel (Bio-Rad, catalog #4561033). Electrophoresis
655 was performed in 1x tris glycine running buffer at 200 V and 4°C for approximately 1 h. Gels were then
656 incubated at room temperature (RT) in the dark for 1 h in 50 mL NBT staining solution (50 mM
657 potassium phosphate, 30 µM riboflavin, 0.48 mM nitro blue tetrazolium chloride, pH 7.8) while shaking
658 at 60 rpm. NBT staining solution was decanted and gels were soaked in diH_2O in the light for
659 approximately 30 min before imaging on an iBright 1500 FL Imager (Thermo Fisher Scientific).
660

661 **Infection experiments**

662 We used the murine inhalation model of cryptococcosis [64] to assess fungal survival and host
663 response after lung infection. For each strain, 5 female A/J mice were used. Mice were anesthetized by
664 isoflurane inhalation and intranasally inoculated with 1 x 10^5 fungal cells of PBS-washed overnight
665 cultures (~18 h) of indicated strains grown in SC. Mice were sacrificed at 14 days post infection and the
666 mouse lung harvested, weighed, and homogenized in cold PBS. Colony forming units (CFU) were
667 calculated by quantitative culture and are represented as CFU/lung. For Histopathology at 14 days post
668 infection, mice were sacrificed using a lethal dose of pentobarbital sodium, and lungs were fixed via
669 intratracheal instillation of neutral buffered formalin under gravity flow [65]. Fixed lungs were submitted

670 to the Immunohistopathology Core at Duke University for paraffin embedding and staining with
671 hematoxylin and eosin.
672
673 **Quantification of infection area in mouse lung sections**
674 Whole images of the hematoxylin and eosin-stained mouse lung sections were obtained on a
675 Keyence BZ-1000 in a 20x tile scan and stitched using Keyence Analysis software. Images were exported
676 as OME TIFFs and passed through 'bfconvert' from the Bio-Formats command line tool (v. 8.3.0) to
677 create image resolution pyramids. Images were then imported into QuPath (v. 0.6.0) for the remainder
678 of analysis. Image scales were corroborated and 18 training regions were taken from the sample set of
679 15 slides to train a pixel classifier. Classes were used to identify 'lung' area vs. 'non-lung' and other
680 structures. The entirety of the image was passed to the pixel classifier to identify the entirety of the lung
681 area. This area was trimmed for mis-identification regions then passed to the classifier to add area
682 measurements of defined classes, obtaining an area (m^2) of lung parenchymal tissue excluding regions of
683 blood and glass. In a blinded manner, samples were annotated for areas of infection based on the
684 presence of (1) interstitial thickening, infiltration and distortion, (2) lymphocyte aggregates, and (3)
685 bronchial/vessel cuffing with infiltrating cells. These annotation regions were then passed to the pixel
686 classifier to calculate the area (m^2) of lung parenchymal tissue within the infected regions. The
687 infected/inflamed area divided by the total area of lung parenchyma yields the ratio of infection
688 restriction.

689 **Processing lung tissue for single cell suspension for flow cytometry analysis**

690 To prepare lung samples, mice were infected with yeast cells as described above and sacrificed
691 at 14 days post infection. Lung cell harvest was performed as described previously [66]. Briefly, lungs
692 were harvested, weighted and placed in 5 mL of lung digestion buffer (1x HBSS, 5% HI-FBS, 10 mM

693 HEPES pH 7.2-7.4, 60 ug/mL Liberase (Roche, Cat# 5401119001), 6.5x 10^3U/mL DNAseI (Millipore, Cat#
694 260913-10MU) and incubated for 25 min at 37°C and 225 rpm. Then, cells were passed through a pre-
695 wetted (1x PBS+0.5% BSA) 70 µm mesh filter. Filtered cells were spun for 5 min (500 xg, 4°C) and
696 supernatant was removed by decanting. The cell pellet was resuspended in 2 mL of hemolysis buffer
697 (0.15 M ammonium chloride, 10 mM potassium bicarbonate, 1 mM EDTA , pH 7.2-7.4) and incubated at
698 RT for 5 min. After incubation, the cell solution was neutralized by the addition of 10 mL 1x PBS to stop
699 hemolysis and cells were pelleted (5 min, 500 xg, 4°C). Cells were resuspended in 1 mL 1x PBS+ 0.5% BSA
700 and filtered through a pre-wetted 70 µm mesh filter as described above. The mesh filter was washed 2x
701 with 1 mL 1x PBS + 0.5% BSA for a total volume of 3 mL per sample . Freshly isolated cells were used for
702 all flow cytometry analysis, unless otherwise noted.

703 **Antibody staining for flow cytometry**

704 For antibody staining, optimal cell density was determined by counting cells using a
705 hemocytometer. Roughly 10^6 cells per sample were analyzed. Cells were blocked using a 1:200 dilution
706 of FC Block antibody (CD16/32, BioLegend Cat#101302) for at least 15 min before antibody staining.
707 Antibodies used for flow cytometry analysis are listed in **Table S5.** Cells were incubated with antibodies
708 for at least 15 min in the dark at RT, then washed with 1x PBS + 0.5% BSA (5min, 500 xg, 4°C). Cells were
709 resuspended in resuspension buffer (for 1 sample: 5 uL Precision Counting Beads (BioLegend,
710 Cat#424902), 1 uL DNAseI (Millipore, Cat# 260913-10MU), 94 uL 1x PBS + 0.5% BSA).

711

712 **Intracellular cytokine staining for flow cytometry**

713 Single cell suspension were prepared from infected lungs as described above. To enhance
714 cytokine production and detection, cells were plated to 2-3 x 10^6 cells in 300 µL of cRPMI and 200 µL of
715 2.5x Phorbol-12-myristate-13-acetate (PMA)/ionomycin in cRPMI was added to cells (final

716 concentrations per well: PMA (Millipore Sigma) 0.1 µg/mL; Ionomycin calcium salt(Adipogen) 0.375
717 µg/mL). Cells were incubated with the PMA/ionomycin mix for 30 min at 37°C and 5% CO_2. Then,
718 Brefeldin A (BioLegend-1x) was added to the cells and cells were incubated for up to 4 h at 37°C and 5%
719 CO_2. Following the 4 h incubation, cells were spun down (500 xg, 4°C, 5 min) and 250 µL of cell
720 supernatant was removed. Then, cells were resuspended in 200 µL of residual media and transferred to
721 a fresh staining plate. To assess cytokine production, cells were first stained with a mix containing Fc
722 block (CD16/32, BioLegend, 1:200 dilution) and fixable LIVE/DEAD Zombie (ThermoFisher Scientific,
723 1:2000 dilution) for 10 min at 4°C in the dark. Extracellular staining followed for 30 min at 4°C in the
724 dark. Next, cells were permeabilized and fixed with the Cyto-Fast Fix Perm Buffer Set (BioLegend) for
725 intracellular cytokine staining following the manufacturer's protocol. Briefly, cells were fixed by addition
726 of 100 µL Cyto-Fast Fix Perm Buffer Set (BioLegend) at RT for 20 min. After fixation, cells were spun
727 down (500 xg, 4°C, 5 min) and washed with perm/wash buffer (Cyto-Fast Fix Perm Buffer Set
728 (BioLegend) ; 100 µL/well). Intracellular antibody staining was performed by adding 50 µL of antibody
729 dilution in perm/wash buffer to the cells. Antibodies used for intracellular staining are listed in **Table S5**.
730 The intracellular staining was performed in the dark at 4°C over night. Next day, cells were spun down
731 (500 xg, 4°C, 5 min) to remove staining solution and washed with 100 µL of perm/wash buffer per well.
732 The washed cells were resuspended in 100 µl 1x PBS.

733 **Flow cytometry analysis**

734 The following markers were used to identify cell populations in the lungs: myeloid cells ($CD45^+$,
735 $CD11b^+$), neutrophils ($CD45^+$, $CD11b^+$, $Ly6G^+$), monocytes ($CD45^+$, $CD11b^+$, $Ly6G^-$, $Ly6C^+$), macrophages
736 ($CD45^+$, $CD11b^+$, $Ly6G^-$, $CD64^+$, $CD24^-$), exudate macrophages ($CD45^+$, $CD11b^+$, $Ly6G^-$, $CD64^+$, $CD24^-$, $Ly6C^+$,
737 Siglec-F^-), interstitial macrophages ($CD45^+$, $CD11b^+$, $Ly6G^-$, $CD64^+$, $CD24^-$, $Ly6C^-$, Siglec-F^-), alveolar
738 macrophages ($CD45^+$, $CD11b^+$, $Ly6G^-$, $CD64^+$, $CD24^-$, $Ly6C^-$, $SiglecF^+$), eosinophils ($CD45^+$, $CD11b^+$, $Ly6G^-$,
739 $CD24^+$, IA-IE^-, $SiglecF^+$), dendritic cells ($CD45^+$, $CD11b^+$, $Ly6G^-$, $CD24^+$, IA-IE^+, DC), lymphocytes ($CD45^+$,

740 CD11b$^-$), B cells (CD45$^+$, CD19$^+$, TCRβ$^-$, CD11b$^-$), T cells (CD45$^+$, TCRβ$^+$, CD3ε$^+$, CD19$^-$, CD11b$^-$), CD4$^+$ T cells
741 (CD45$^+$, TCRβ$^+$, CD3ε$^+$, CD4$^+$, CD19$^-$, CD11b$^-$), CD8$^+$ T cells (CD45$^+$, TCRβ$^+$, CD3ε$^+$, CD8$^+$, CD19$^-$, CD11b$^-$), γδ T
742 cells (CD45$^+$, TCRβ$^-$, CD19$^-$, CD11b$^-$, CD3ε$^+$, γδTCR$^+$). Intracellular cytokines markers: IFNγ, IL-17A, and IL-4.
743 Data was acquired on the Cytek Aurora (Cytek Biosciences) and data analyses was performed using Flow
744 Jo (TreeStar).

745

746 **Statistical analysis**

747 All data error bars represent standard errors of the means (SEM) of results from a number of
748 biological replicates (N), as indicated in figure legends. Prior to statistical analysis, data from all
749 experiments was $\log_2$ transformed for comparison of proportions. Statistical analysis was conducted
750 using GraphPad Prism software v9. The statistical tests used in each experiment and their results (i.e., p
751 values) are indicated in figure legends. Asterisks in figures correspond to statistical significance as
752 follows: ****, $P < 0.0001$; ***, $P = 0.0001$ to $P < 0.001$; **, $P = 0.001$ to $P < 0.01$; *, $P = 0.01$ to $P < 0.05$;
753 ns (not significant), $P > 0.05$.

754

755 Acknowledgements

756 We thank the Duke Immunohistopathology Core for preparation and staining of the infected lung tissue.
757 Research reported in this publication was supported by the National Institute of General Medical
758 Sciences of the National Institutes of Health under award number R01GM145035 (C.D.J. and K.J.F.) and
759 R01GM041840 (J.A.A. and C.P.) and by the National Institute Of Allergy And Infectious Diseases of the
760 National Institutes of Health under award number R01AI184401 (J.A.A., C.P. and M.L.S) The content is
761 solely the responsibility of the authors and does not necessarily represent the official views of the

National Institutes of Health. J.A.A. and C.P. acknowledge further support by Duke University School of Medicine Bridge Funding 4532750. C.A.D.J received fellowship support from the Tri-Institutional Molecular Mycology and Pathogenesis Training Program (T32-AI052080).

FIGURE LEGENDS

Figure 1: Comparison of single versus dual fungal Cu-sensing transcription factors.

(A) Mode of action of single Cu-sensing TFs found in model ascomycetes versus the dual Cu-sensing TF in *Cn*. Both systems use a highly conserved DNA binding motif to bind target promoter sequences (highlighted in yellow). Cu binding to Cys-rich motifs encoded by single Cu-sensing TFs results in confirmational changes, which either inhibit transcriptional activity of low Cu-responsive Mac1-like TFs (orange) or activate transcriptional activity of high Cu-responsive Ace1-like TFs (blue). In contrast, *Cn* uses only one Cu-responsive TF, *Cn*Cuf1 (green), which must remain transcriptionally active during low and high Cu stress but is directed to distinct promoter regions based on variance of cellular Cu levels. Motifs involved in Cu-sensing and regulating *Cn*Cuf1 transcriptional activity are yet unknown. **(B)** Schematic representation of the *Cn*Cuf1 domain structure and conserved motifs. The first and last residues of each domain are indicated. The N-terminal domain is shown in light grey; the C-terminal domain is shown in dark grey. The N-terminal DNA binding motif, which contains the conserved KGRP DNA binding motif, is highlighted in yellow. The Ace1-like cysteine-rich region is indicated via a blue box, and the Mac1-like regions are indicated by an orange box. The sequence of the identified cysteines (Cys, C) is indicated for each region; the *Cn*Cuf1-unique Cys-rich sequence located adjacent to the 2nd Mac1-like Cys-rich motif is highlighted in turquoise.

785 **Figure 2: The Cuf1-FLAG ΔAce1 mutant protein is produced to WT levels but fails to restore growth**
786 **during high Cu stress.**

787 **(A)** Cuf1-FLAG WT, Cuf1-FLAG KGRP-AAAA, Cuf1-FLAG ΔAce1 and Cuf1-FLAG ΔMac1 mutant protein
788 expression assessed by western blot analysis. Indicated *CUF1-FLAG* expressing strains were incubated in
789 SC medium supplemented with either 1 mM $CuSO_4$ or 1 mM BCS at a starting OD_{600} of 0.5 for 3 h at
790 30°C. A TCA based protein extraction was performed. 25 µL of crude TCA extract was analyzed per lane
791 with the α FLAG-HRP conjugate. The α GAPDH (anti-GAPDH) antibody was used as a loading control. **(B)**
792 Growth analysis in the presence of high and low Cu stress. Five-fold serial dilutions of cell suspensions
793 for each strain were spotted onto SC medium agar plates. To induce low Cu stress, the SC medium was
794 supplemented with 0.5 or 1 mM BCS. To induce varying degrees of high Cu stress, the SC medium was
795 supplemented with either 0.02, 0.05, 0.1, 0.25 or 1 mM $CuSO_4$. Plates were incubated at 30°C for 3 days.
796 Two independent strains of each *CUF1-FLAG* mutant were analyzed. As Cu stress controls, the Cu import
797 mutant *ctr1*Δ *ctr4*Δ and the Cu detoxification mutant *cmt1*Δ *cmt2*Δ were included in the growth analysis.
798 **(C)** Cuf1-FLAG WT, Cuf1-FLAG Δ181, Cuf1-FLAG Δ338, Cuf1-FLAG Δ410, Cuf1-FLAG Δ513 and Cuf1-FLAG
799 Δ780 protein fragment expression assessed by western blot analysis. Indicated *CUF1-FLAG* expressing
800 strains were incubated in SC medium supplemented with either 1 mM $CuSO_4$ or 1 mM BCS at a starting
801 OD_{600} of 0.5 for 3 h at 30°C. Protein extraction and western blot was performed as described in (A). **(D)**
802 Growth analysis in the presence of high and low Cu stress. Five-fold serial dilutions of cell suspensions
803 for each strain were spotted onto SC medium agar plates. Indicated strains were spotted on to Cu stress
804 plates as described in (B).

805

806 **Figure 3: Mutation of the Ace1-like Cys-rich motif renders Cuf1 unable to bind to and activate high Cu**
807 **regulated genes.**

808 **(A)** p*CTR4*-m*CLOVER* and p*CMT1*-m*RUBY* expression profiles of *CUF1-FLAG* WT and site mutant
809 expressing strains**.** Indicated strains were inoculated to OD_{600} of 0.1 into SC + 50 µM BCS or SC + 50 µM
810 $CuSO_4$ and grown for 24 h at 30°C. A TCA based protein extraction was performed and 20 µg total
811 protein was analyzed per lane. mClover was detected using a monoclonal anti-GFP antibody (mouse,
812 αGFP) and mRuby was detected using a polyclonal anti-RFP antibody (rabbit, αRFP). An anti-GAPDH
813 antibody (rabbit, αGAPDH) was used as a loading control. **(B-C)** Transcript abundance of the low Cu-
814 regulated *CTR4* and *CBI1* genes (B) and the high Cu-regulated *CMT1* and *AMT1* genes (C). Indicated
815 strains were diluted to OD_{600} of 0.5 and incubated for 2 h at 30°C in SC medium. Cu stress was induced
816 by the addition of either 1 mM BCS or 1 mM $CuSO_4$ and cultures were incubated for 3 h at 30°C.
817 Transcript abundance for each indicated gene was assessed by quantitative real-time PCR (qPCR), and
818 the $\log_2$ fold change of transcripts was calculated using the $\Delta\Delta C_T$ method in low Cu stress versus high Cu
819 stress (B) or high Cu stress versus low Cu stress (C). Transcript levels were normalized to *GAPDH*. Shown
820 is the mean +/- SEM of 4 biological replicates. Statistical analysis was performed using one-way ANOVA.
821 **(D-E)** Cuf1-FLAG promoter binding at low Cu stress (D) or high Cu stress (E). Indicated strains were
822 diluted to OD_{600} of 0.25 and incubated for 2 h at 30°C in SC medium. Cu stress was induced by the
823 addition of either 1 mM BCS or 1 mM $CuSO_4$, and cultures were incubated for 2.5 h at 30°C prior to
824 crosslinking. Promoter binding to the target promoters was analyzed via (ChIP-PCR). Fold enrichment
825 was calculated by comparison of target promoter abundance in the FLAG-tagged strains to the promoter
826 abundance in the non-FLAG tagged, WT strain. The mean +/- SEM of 3 biological replicates is shown. A
827 two-tailed t-test was performed as statistical analysis.
828

829 **Figure 4: Cuf1 Ace1-like Cys-rich motif is essential for *LAC1* regulation in response to excess copper.**

830 **(A)** Schematic summary of the role of Cu and Cuf1 regulation of Lac1 activity and melanin production
831 during both Cu limitation and Cu excess. In the absence of Cuf1-induction of Cu-import genes during Cu
832 limitation, melanin production by Lac1 is impaired. Cuf1 is also required for expression of the *LAC1* gene
833 during Cu excess. Images made using BioRender. **(B)** Melanization during Cu limitation (10 µM BCS) and
834 in presence of exogenous copper (10 µM $CuSO_4$). Indicated strains were grown for 18 h in SC at 30°C,
835 diluted to OD_{600} of 2.5 and spotted onto L-DOPA agar plates with indicated supplementation. L-DOPA
836 plates were incubated for 3 days at 30°C. Melanin production is demonstrated by colony pigmentation
837 **(C-D)** *LAC1* (C) and *CTR4* (D) transcript abundance in melanin-inducing conditions. Indicated strains were
838 diluted to OD_{600} of 0.5 in liquid L-DOPA medium supplemented with either 10 µM BCS or 10 µM $CuSO_4$
839 and grown for 3 h at 30°C. Relative transcript abundance for *LAC1* (C) or *CTR4* (D) was assessed by
840 quantitative RT-PCR and normalized to WT transcript levels via the $\Delta\Delta C_T$ method. The data is presented
841 as the mean +/- SEM of the $\log_2$ fold change of 3 biological replicates. Statistical analysis was performed
842 using a one-way ANOVA.

843

844 **Figure 5: Cuf1 Ace1-like Cys-rich motif is required for superoxide dismutase (Sod)-dependent ROS**
845 **detoxification during high Cu stress.**

846 **(A)** Schematic summary of the role of Cu and Cuf1 for Sod protein regulation during Cu limitation and
847 excess. Cu, Zn-containing Sod1 is the major cytosolic Sod in Cu sufficiency and excess. The mitochondrial
848 Mn-dependent Sod2 assumes the majority of cytosolic Sod function during Cu limitation. Images were
849 made using BioRender. **(B-C)** Disc diffusion assay to test cellular superoxide sensitivity. Indicated strains
850 were inoculated on SC agar plates supplemented with indicated amounts of BCS or $CuSO_4$. Cells were
851 challenged with increasing concentrations of the superoxide generator menadione on filter discs as
852 depicted in (B) for 3 days at 30°C (C). **(D)** In-gel SOD activity assays from whole cell extracts of indicated

853 strains. For Cu stress induction, strains were incubated in SC medium supplemented with indicated
854 amounts of BCS or $CuSO_4$ for 24 h at 30°C. Whole cell extracts were generated, separated by native
855 PAGE, and stained for SOD activity using nitroblue tetrazolium (NBT) staining solution. **(E)** Transcript
856 abundance of the *SOD1* gene during high Cu and low Cu stress. Indicated strains were diluted to OD_{600}
857 0.5 and incubated for 2 h at 30°C in SC medium. Cu stress was induced by the addition of either 1 mM
858 BCS or 1 mM $CuSO_4$ and cultures were incubated for 3 h at 30°C. Relative transcript abundance for *SOD1*
859 was assessed by quantitative RT-PCR and normalized to WT transcript levels using the $\Delta\Delta C_T$ method. The
860 data is presented as the mean +/- SEM of the $\log_2$ fold change of 3 biological replicates and statistical
861 analysis was performed using a one-way ANOVA.

862

863 **Figure 6: Effects of Cuf1 high Cu stress regulation on survival, yeast cell dissemination and**
864 **inflammation in the infected mouse lung.**

865 Intranasal infection of female A/J mice. Mice were infected by inhalation with 10^5 cells of the indicated
866 strains (5 mice/strain). Mice were sacrificed 14 days postinfection and their lungs harvested. **(A-C)** Lung
867 fungal burden 14 days postinfection. Lung lysates were assessed by quantitative culture (A), lung wet
868 weight (B) and macroscopic lung abnormalities (C). (A-B) Data was plotted, and an unpaired t-test was
869 performed using GraphPad Prism (B only). (C) Foci are indicated with white arrows. **(D-F)** Histopathology
870 analysis of infected murine lungs 14 days post infection. Mice were sacrificed and lungs were fixed via
871 intratracheal instillation of neutral buffered formalin under gravity flow. Hematoxylin and eosin staining
872 were used to visualize microscopic lung pathology. (D) Representative stitched 20x tile scan images used
873 for quantification of infected/inflamed lung area. Infected/inflamed areas are highlighted in yellow. (E)
874 Quantification plot of infected versus non-infected section area using stitched 20x images. Plot was
875 generated via GraphPad prism and a Welch's t-Test with unequal sample sizes was performed. (F)

876 Representative 4x and 20x images. Yeast enriched foci of inflammation are highlighted by a black
877 arrowhead. The length of the black bar represents 250 µm.

878

879 **References**

880 1. Maret W. The Metals in the Biological Periodic System of the Elements: Concepts and
881 Conjectures. *International journal of molecular sciences*. 2016;17(1). Epub 2016/01/08. doi:
882 10.3390/ijms17010066.

883 2. Smith AD, Logeman BL, Thiele DJ. Copper Acquisition and Utilization in Fungi. *Annual review of*
884 *microbiology*. 2017;71:597-623. Epub 2017/09/10. doi: 10.1146/annurev-micro-030117-020444.

885 3. Halliwell B, Gutteridge JM. The importance of free radicals and catalytic metal ions in human
886 diseases. *Molecular aspects of medicine*. 1985;8(2):89-193. Epub 1985/01/01. doi: 10.1016/0098-
887 2997(85)90001-9.

888 4. Giachino A, Waldron KJ. Copper tolerance in bacteria requires the activation of multiple
889 accessory pathways. *Molecular microbiology*. 2020;114(3):377-90. doi:
890 https://doi.org/10.1111/mmi.14522.

891 5. Robison ATR, Sturrock GR, Zaengle-Barone JM, Wiebelhaus N, Dharani A, Williams IG, *et al.*
892 Analysis of copper-induced protein precipitation across the *E. coli* proteome. *Metallomics : integrated*
893 *biometal science*. 2023;15(1). Epub 2022/12/23. doi: 10.1093/mtomcs/mfac098.

894 6. Zuily L, Lahrach N, Fassler R, Genest O, Faller P, Sénèque O, *et al*. Copper Induces Protein
895 Aggregation, a Toxic Process Compensated by Molecular Chaperones. *mBio*. 2022;13(2):e0325121. Epub
896 2022/03/16. doi: 10.1128/mbio.03251-21.

897 7. Macomber L, Imlay JA. The iron-sulfur clusters of dehydratases are primary intracellular targets
898 of copper toxicity. *Proceedings of the National Academy of Sciences of the United States of America*.
899 2009;106(20):8344-9. Epub 2009/05/07. doi: 10.1073/pnas.0812808106.
900 8. Imlay JA. The mismetallation of enzymes during oxidative stress. *The Journal of biological*
901 *chemistry.* 2014;289(41):28121-8. Epub 2014/08/28. doi: 10.1074/jbc.R114.588814.
902 9. Merchant SS, Schmollinger S, Strenkert D, Moseley JL, Blaby-Haas CE. From economy to luxury:
903 Copper homeostasis in Chlamydomonas and other algae. *Biochimica et biophysica acta Molecular cell*
904 *research*. 2020;1867(11):118822. Epub 2020/08/18. doi: 10.1016/j.bbamcr.2020.118822.
905 10. Li CX, Gleason JE, Zhang SX, Bruno VM, Cormack BP, Culotta VC. *Candida albicans* adapts to host
906 copper during infection by swapping metal cofactors for superoxide dismutase. *Proceedings of the*
907 *National Academy of Sciences of the United States of America*. 2015;112(38):E5336-42. Epub
908 2015/09/10. doi: 10.1073/pnas.1513447112.
909 11. Smith AD, Garcia-Santamarina S, Ralle M, Loiselle DR, Haystead TA, Thiele DJ. Transcription
910 factor-driven alternative localization of *Cryptococcus neoformans* superoxide dismutase. *The Journal of*
911 *biological chemistry*. 2021;296:100391. Epub 2021/02/11. doi: 10.1016/j.jbc.2021.100391.
912 12. Ray SC, Rappleye CA. Mac1-Dependent Copper Sensing Promotes *Histoplasma* Adaptation to the
913 Phagosome during Adaptive Immunity. *mBio*. 2022;13(2):e03773-21. doi: doi:10.1128/mbio.03773-21.
914 13. Mohamed SH, Fu MS, Hain S, Alselami A, Vanhoffelen E, Li Y, *et al*. Microglia are not protective
915 against *cryptococcal* meningitis. *Nat Commun*. 2023;14(1):7202. Epub 2023/11/08. doi: 10.1038/s41467-
916 023-43061-0.
917 14. García-Santamarina S, Thiele DJ. Copper at the Fungal Pathogen-Host Axis. *The Journal of*
918 *biological chemistry*. 2015;290(31):18945-53. Epub 2015/06/10. doi: 10.1074/jbc.R115.649129.

919 15. Murdoch CC, Skaar EP. Nutritional immunity: the battle for nutrient metals at the host–
920 pathogen interface. *Nature Reviews Microbiology*. 2022;20(11):657-70. doi: 10.1038/s41579-022-00745-
921 6.
922 16. Besold Angelique N, Gilston Benjamin A, Radin Jana N, Ramsoomair C, Culbertson Edward M, Li
923 Cissy X, et al. Role of Calprotectin in Withholding Zinc and Copper from *Candida albicans*. *Infection and*
924 *Immunity*. 2018;86(2):10.1128/iai.00779-17. doi: 10.1128/iai.00779-17.
925 17. Garg R, David MS, Yang S, Culotta VC. Metals at the Host–Fungal Pathogen Battleground. *Annual*
926 *Review Microbiology*. 2024;78(Volume 78, 2024):23-38. doi: https://doi.org/10.1146/annurev-micro-
927 041222-023745.
928 18. White C, Lee J, Kambe T, Fritsche K, Petris MJ. A role for the ATP7A copper-transporting ATPase
929 in macrophage bactericidal activity. *The Journal of biological chemistry.* 2009;284(49):33949-56. Epub
930 2009/10/08. doi: 10.1074/jbc.M109.070201.
931 19. Rajasingham R, Smith RM, Park BJ, Jarvis JN, Govender NP, Chiller TM, *et al*. Global burden of
932 disease of HIV-associated *cryptococcal* meningitis: an updated analysis. *The Lancet Infectious diseases.*
933 2017;17(8):873-81. Epub 2017/05/10. doi: 10.1016/s1473-3099(17)30243-8.
934 20. Heitman J, Kozel TR, Kwon-Chung KJ, Perfect JR, Casadevall A. *Cryptococcus* : from human
935 pathogen to model yeast. Washington, DC: *ASM Press*; 2011.
936 http://www.asmscience.org/content/book/10.1128/9781555816858.
937 21. Ding C, Festa RA, Chen YL, Espart A, Palacios Ò, Espín J, *et al*. *Cryptococcus neoformans* copper
938 detoxification machinery is critical for fungal virulence. *Cell host & microbe*. 2013;13(3):265-76. Epub
939 2013/03/19. doi: 10.1016/j.chom.2013.02.002.
940 22. Sun TS, Ju X, Gao HL, Wang T, Thiele DJ, Li JY, *et al*. Reciprocal functions of *Cryptococcus*
941 *neoformans* copper homeostasis machinery during pulmonary infection and meningoencephalitis. *Nat*
942 *Commun.* 2014;5:5550. Epub 2014/11/25. doi: 10.1038/ncomms6550.

943 23. Garcia-Santamarina S, Festa RA, Smith AD, Yu CH, Probst C, Ding C, *et al.* Genome-wide analysis
944 of the regulation of Cu metabolism in *Cryptococcus neoformans*. *Molecular microbiology.*
945 2018;108(5):473-94. Epub 2018/04/03. doi: 10.1111/mmi.13960.
946 24. Garcia-Santamarina S, Uzarska MA, Festa RA, Lill R, Thiele DJ. *Cryptococcus neoformans* Iron-
947 Sulfur Protein Biogenesis Machinery Is a Novel Layer of Protection against Cu Stress. *mBio*. 2017;8(5).
948 Epub 2017/11/02. doi: 10.1128/mBio.01742-17.
949 25. Do E, Park S, Li MH, Wang JM, Ding C, Kronstad JW, *et al*. The mitochondrial ABC transporter
950 Atm1 plays a role in iron metabolism and virulence in the human fungal pathogen *Cryptococcus*
951 *neoformans. Medical mycology*. 2018;56(4):458-68. Epub 2018/02/09. doi: 10.1093/mmy/myx073.
952 PubMed
953 26. Cox GM, Harrison TS, McDade HC, Taborda CP, Heinrich G, Casadevall A, *et al.* Superoxide
954 dismutase influences the virulence of *Cryptococcus neoformans* by affecting growth within
955 macrophages. *Infect Immun*. 2003;71(1):173-80. Epub 2002/12/24. doi: 10.1128/iai.71.1.173-180.2003.
956 27. Probst C, Garcia-Santamarina S, Brooks JT, Van Der Kloet I, Baars O, Ralle M, *et al*. Interactions
957 between copper homeostasis and the fungal cell wall affect copper stress resistance. *PLoS pathogens*.
958 2022;18(6):e1010195. Epub 2022/06/24. doi: 10.1371/journal.ppat.1010195.
959 28. Garcia-Santamarina S, Probst C, Festa RA, Ding C, Smith AD, Conklin SE, *et al.* A lytic
960 polysaccharide monooxygenase-like protein functions in fungal copper import and meningitis. *Nature*
961 *chemical biology*. 2020;16(3):337-44. Epub 2020/01/15. doi: 10.1038/s41589-019-0437-9.
962 29. Thiele DJ. *ACE1* regulates expression of the *Saccharomyces cerevisiae* metallothionein gene.
963 *Molecular and cellular biology*. 1988;8(7):2745-52. Epub 1988/07/01. doi: 10.1128/mcb.8.7.2745-
964 2752.1988.
965 30. Culotta VC, Hsu T, Hu S, Fürst P, Hamer D. Copper and the *ACE1* regulatory protein reversibly
966 induce yeast metallothionein gene transcription in a mouse extract. *Proceedings of the National*

967 *Academy of Sciences of the United States of America.* 1989;86(21):8377-81. Epub 1989/11/01. doi:
968 10.1073/pnas.86.21.8377.
969 31. Jungmann J, Reins HA, Lee J, Romeo A, Hassett R, Kosman D, *et al*. *MAC1*, a nuclear regulatory
970 protein related to Cu-dependent transcription factors is involved in Cu/Fe utilization and stress
971 resistance in yeast. *The EMBO journal*. 1993;12(13):5051-6. Epub 1993/12/15. doi: 10.1002/j.1460-
972 2075.1993.tb06198.x.
973 32. Waterman SR, Hacham M, Hu G, Zhu X, Park YD, Shin S, *et al*. Role of a *CUF1/CTR4* copper
974 regulatory axis in the virulence of *Cryptococcus neoformans*. *The Journal of clinical investigation*.
975 2007;117(3):794-802. Epub 2007/02/10. doi: 10.1172/jci30006.
976 33. Beaudoin J, Mercier A, Langlois R, Labbé S. The *Schizosaccharomyces pombe* Cuf1 is composed
977 of functional modules from two distinct classes of copper metalloregulatory transcription factors. *The*
978 *Journal of biological chemistry.* 2003;278(16):14565-77. Epub 2003/02/13. doi:
979 10.1074/jbc.M300861200.
980 34. Beaudoin J, Labbé S. Copper Induces Cytoplasmic Retention of Fission Yeast Transcription Factor
981 Cuf1. *Eukaryot Cell*. 2006;5(2):277-92. doi: doi:10.1128/ec.5.2.277-292.2006.
982 35. Szczypka MS, Thiele DJ. A cysteine-rich nuclear protein activates yeast metallothionein gene
983 transcription. *Molecular and cellular biology*. 1989;9(2):421-9. Epub 1989/02/01. doi:
984 10.1128/mcb.9.2.421-429.1989
985 36. Graden JA, Posewitz MC, Simon JR, George GN, Pickering IJ, Winge DR. Presence of a copper(I)-
986 thiolate regulatory domain in the copper-activated transcription factor Amt1. *Biochemistry*.
987 1996;35(46):14583-9. Epub 1996/11/19. doi: 10.1021/bi961642v.
988 37. Koch KA, Thiele DJ. Autoactivation by a *Candida glabrata* copper metalloregulatory transcription
989 factor requires critical minor groove interactions. *Molecular and cellular biology*. 1996;16(2):724-34.
990 Epub 1996/02/01. doi: 10.1128/mcb.16.2.724.

991 38. Serpe M, Joshi A, Kosman DJ. Structure-function analysis of the protein-binding domains of
992 Mac1p, a copper-dependent transcriptional activator of copper uptake in *Saccharomyces cerevisiae*. *The*
993 *Journal of biological chemistry*. 1999;274(41):29211-9. Epub 1999/10/03. doi:
994 10.1074/jbc.274.41.29211.
995 39. Fürst P, Hu S, Hackett R, Hamer D. Copper activates metallothionein gene transcription by
996 altering the conformation of a specific DNA binding protein. *Cell*. 1988;55(4):705-17. Epub 1988/11/18.
997 doi: 10.1016/0092-8674(88)90229-2.
998 40. Arras SD, Chitty JL, Blake KL, Schulz BL, Fraser JA. A genomic safe haven for mutant
999 complementation in *Cryptococcus neoformans*. *PloS one*. 2015;10(4):e0122916. Epub 2015/04/10. doi:
1000 10.1371/journal.pone.0122916.
1001 41. Upadhya R, Lam WC, Maybruck BT, Donlin MJ, Chang AL, Kayode S, *et al*. A fluorogenic *C.*
1002 *neoformans* reporter strain with a robust expression of m-cherry expressed from a safe haven site in the
1003 genome. *Fungal genetics and biology : FG & B.* 2017;108:13-25. Epub 2017/09/06. doi:
1004 10.1016/j.fgb.2017.08.008.
1005 42. Camacho E, Vij R, Chrissian C, Prados-Rosales R, Gil D, O'Meally RN, *et al.* The structural unit of
1006 melanin in the cell wall of the fungal pathogen *Cryptococcus neoformans*. *The Journal of biological*
1007 *chemistry*. 2019;294(27):10471-89. Epub 2019/05/24. doi: 10.1074/jbc.RA119.008684.
1008 43. Zhu X, Williamson PR. Role of laccase in the biology and virulence of *Cryptococcus neoformans*.
1009 *FEMS Yeast Research*. 2004;5(1):1-10. doi: 10.1016/j.femsyr.2004.04.004 %J FEMS Yeast Research.
1010 44. Jiang N, Sun N, Xiao D, Pan J, Wang Y, Zhu X. A copper-responsive factor gene *CUF1* is required
1011 for copper induction of laccase in *Cryptococcus neoformans*. *FEMS Microbiol Lett*. 2009;296(1):84-90.
1012 Epub 2009/05/23. doi: 10.1111/j.1574-6968.2009.01619.x.
1013 45. Xue P, Hu G, Jung WH, Kronstad JW. Metals and the cell surface of *Cryptococcus neoformans*.
1014 *Current Opinion in Microbiology*. 2023;74:102331. doi: https://doi.org/10.1016/j.mib.2023.102331.

1015 46. Ding C, Yin J, Tovar EMM, Fitzpatrick DA, Higgins DG, Thiele DJ. The copper regulon of the
1016 human fungal pathogen *Cryptococcus neoformans* H99. *Mol Microbiol*. 2011;81(6):1560-76. doi:
1017 https://doi.org/10.1111/j.1365-2958.2011.07794.x.
1018 47. Telzrow CL, Esher Righi S, Castro-Lopez N, Campuzano A, Brooks JT, Carney JM, *et al.* An
1019 Immunogenic and Slow-Growing *Cryptococcal* Strain Induces a Chronic Granulomatous Infection in
1020 Murine Lungs. *Infect Immun*. 2022;90(6):e0058021. Epub 2022/05/20. doi: 10.1128/iai.00580-21.
1021 48. Jensen LT, Winge DR. Identification of a copper-induced intramolecular interaction in the
1022 transcription factor Mac1 from *Saccharomyces cerevisiae. EMBO J*. 1998;17(18):5400-8. Epub
1023 1998/09/16. doi: 10.1093/emboj/17.18.5400.
1024 49. Cai Z, Du W, Zhang Z, Guan L, Zeng Q, Chai Y, et al. The transcription factor AceA is involved not
1025 only in Cu but also in Zn detoxification through regulating transporters CrpA and ZrcA. *Cellular*
1026 *Microbiology*. 2018;20(10):e12864. doi: https://doi.org/10.1111/cmi.12864.
1027 50. Beaudoin J, Labbé S. Crm1-Mediated Nuclear Export of the *Schizosaccharomyces pombe*
1028 Transcription Factor Cuf1 during a Shift from Low to High Copper Concentrations. *Eukaryot Cell*.
1029 2007;6(5):764-75. doi: doi:10.1128/ec.00002-07.
1030 51. Upadhyay S, Torres G, Lin X. Laccases involved in 1,8-dihydroxynaphthalene melanin
1031 biosynthesis in *Aspergillus fumigatus* are regulated by developmental factors and copper homeostasis.
1032 *Eukaryotic cell*. 2013;12(12):1641-52. Epub 2013/10/15. doi: 10.1128/ec.00217-13.
1033 52. Saikia S, Oliveira D, Hu G, Kronstad J. Role of ferric reductases in iron acquisition and virulence in
1034 the fungal pathogen *Cryptococcus neoformans*. *Infect Immun*. 2014;82(2):839-50. Epub 2014/01/31. doi:
1035 10.1128/iai.01357-13.
1036 53. Khemiri I, Tebbji F, Sellam A. Transcriptome Analysis Uncovers a Link Between Copper
1037 Metabolism, and Both Fungal Fitness and Antifungal Sensitivity in the Opportunistic Yeast *Candida*
1038 *albicans*. *Front. Microbiol.* 2020;11. doi: 10.3389/fmicb.2020.00935.

1039 54. Cai Z, Du W, Zeng Q, Long N, Dai C, Lu L. Cu-sensing transcription factor Mac1 coordinates with
1040 the Ctr transporter family to regulate Cu acquisition and virulence in *Aspergillus fumigatus*. *Fungal*
1041 *Genetics and Biology*. 2017;107:31-43. doi: https://doi.org/10.1016/j.fgb.2017.08.003.
1042 55. Ballou ER, Wilson D. The roles of zinc and copper sensing in fungal pathogenesis. *Current*
1043 *Opinion in Microbiology*. 2016;32:128-34. doi: https://doi.org/10.1016/j.mib.2016.05.013.
1044 56. Moraes D, Tristão GB, Rappleye CA, Ray SC, Ribeiro-Dias F, Gomes RS, *et al.* The influence of a
1045 copper efflux pump in *Histoplasma capsulatum* virulence. *The FEBS journal*. 2024;291(4):744-60. Epub
1046 2023/11/11. doi: 10.1111/febs.16999.
1047 57. Ost KS, Esher SK, Leopold Wager CM, Walker L, Wagener J, Munro C, *et al.* Rim Pathway-
1048 Mediated Alterations in the Fungal Cell Wall Influence Immune Recognition and Inflammation. *mBio*.
1049 2017;8(1). doi: https://doi.org/10.1128/mbio.02290-16.
1050 58. Esher SK, Ost KS, Kohlbrenner MA, Pianalto KM, Telzrow CL, Campuzano A, *et al.* Defects in
1051 intracellular trafficking of fungal cell wall synthases lead to aberrant host immune recognition. *PLoS*
1052 *pathogens*. 2018;14(6):e1007126. Epub 2018/06/05. doi: 10.1371/journal.ppat.1007126.
1053 59. Hole CR, Lam WC, Upadhya R, Lodge JK. *Cryptococcus neoformans* Chitin Synthase 3 Plays a
1054 Critical Role in Dampening Host Inflammatory Responses. *mBio*. 2020;11(1):10.1128/mbio.03373-19.
1055 doi: doi:10.1128/mbio.03373-19.
1056 60. Upadhya R, Lam WC, Hole CR, Vasselli JG, Lodge JK. Cell wall composition in *Cryptococcus*
1057 *neoformans* is media dependent and alters host response, inducing protective immunity. *Frontiers in*
1058 *fungal biology*. 2023;4. Epub 2023/08/04. doi: 10.3389/ffunb.2023.1183291.
1059 61. Toffaletti DL, Rude TH, Johnston SA, Durack DT, Perfect JR. Gene transfer in *Cryptococcus*
1060 *neoformans* by use of biolistic delivery of DNA. *Journal of Bacteriology*. 1993;175(5):1405-11. doi:
1061 10.1128/jb.175.5.1405-1411.1993.

1062 62. du Plooy LM, Telzrow CL, Nichols CB, Probst C, Castro-Lopez N, Wormley FL, Jr., *et al*. A fungal
1063 ubiquitin ligase and arrestin binding partner contribute to pathogenesis and survival during cellular
1064 stress. *mBio*. 2024;15(10):e0098124. Epub 2024/09/05. doi: 10.1128/mbio.00981-24.
1065 63. Upadhya R, Probst C, Alspaugh JA, Lodge JK. Measuring Stress Phenotypes in *Cryptococcus*
1066 *neoformans*. *Methods in molecular biology*. 2024;2775:277-303. Epub 2024/05/17. doi: 10.1007/978-1-
1067 0716-3722-7_19.
1068 64. Probst C, Hallas-Møller M, Ipsen J, Brooks JT, Andersen K, Haon M, *et al*. A fungal lytic
1069 polysaccharide monooxygenase is required for cell wall integrity, thermotolerance, and virulence of the
1070 fungal human pathogen *Cryptococcus neoformans*. *PLoS pathogens*. 2023;19(4):e1010946. Epub
1071 2023/04/26. doi: 10.1371/journal.ppat.1010946.
1072 65. Hsia CC, Hyde DM, Ochs M, Weibel ER. An official research policy statement of the American
1073 Thoracic Society/European Respiratory Society: standards for quantitative assessment of lung structure.
1074 *American journal of respiratory and critical care medicine*. 2010;181(4):394-418. Epub 2010/02/05. doi:
1075 10.1164/rccm.200809-1522ST.
1076 66. Xu-Vanpala S, Deerhake ME, Wheaton JD, Parker ME, Juvvadi PR, MacIver N, *et al*. Functional
1077 heterogeneity of alveolar macrophage population based on expression of CXCL2. *Science immunology*.
1078 2020;5(50). Epub 2020/08/10. doi: 10.1126/sciimmunol.aba7350.

1079

A

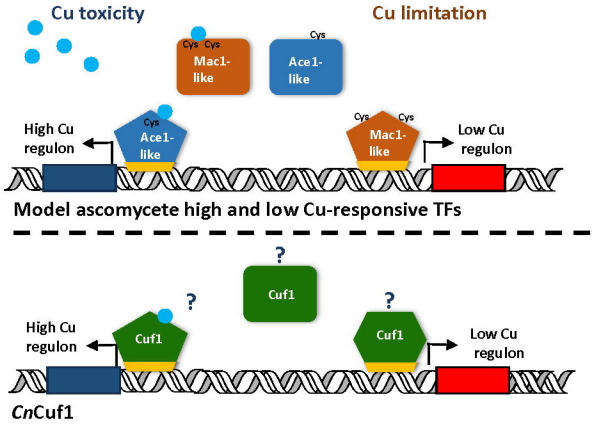
Cu toxicity
Cu limitation
Cys Cys
Mac1-like
Cys
Ace1-like
High Cu regulon
Cys
Ace1-like
Cys Cys
Mac1-like
Low Cu regulon
Model ascomycete high and low Cu-responsive TFs
?
Cuf1
?
?
High Cu regulon
Cuf1
Cuf1
Low Cu regulon
CnCuf1

B

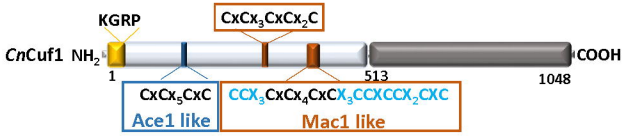
KGRP
CxCx3CxCx2C
CnCuf1 NH2
COOH
1
513
1048
CxCx5CxC
Ace1 like
CCX3CxCx4CxCX3CCXCCX2CXC
Mac1 like

Figure 1

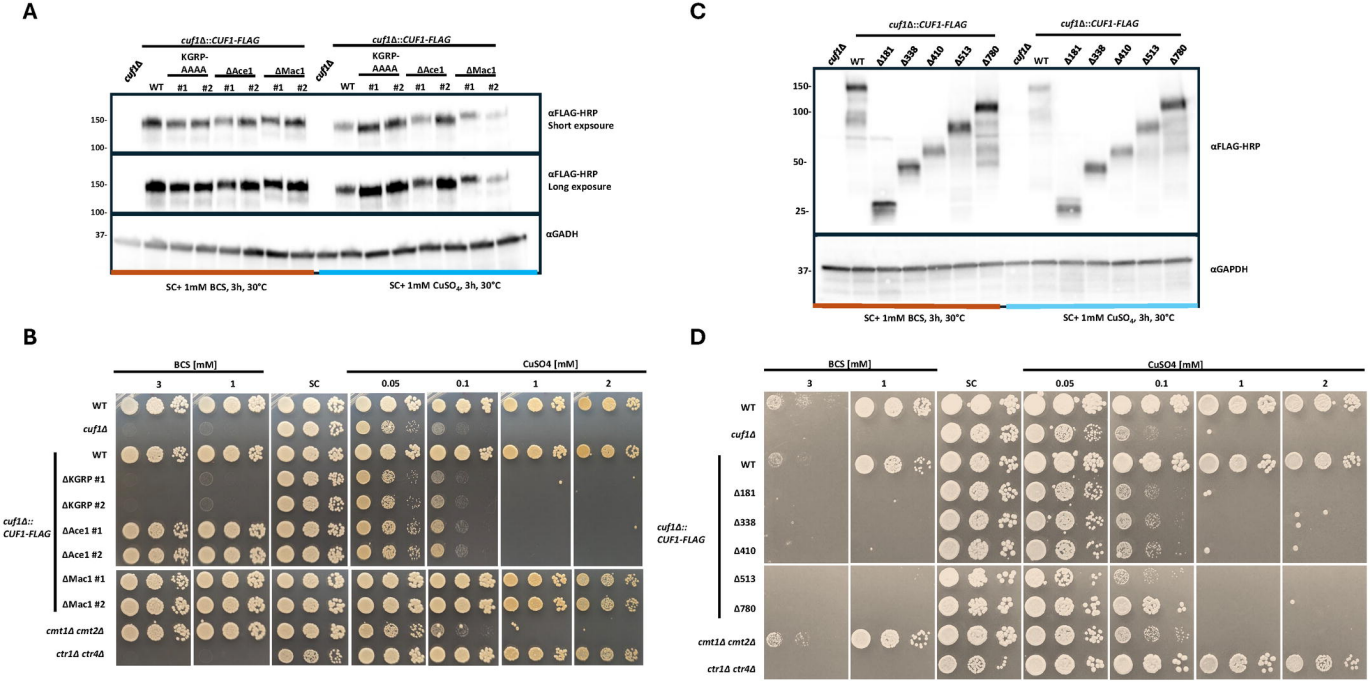
A
cuf1Δ::CUF1-FLAG
cuf1Δ::CUF1-FLAG
cuf1Δ
KGRP-AAAA
ΔAce1
ΔMac1
WT #1 #2 #1 #2 #1 #2
150-
100-
37-
αFLAG-HRP Short expsoure
αFLAG-HRP Long exposure
αGADH
SC+ 1mM BCS, 3h, 30°C
SC+ 1mM CuSO4, 3h, 30°C
B
BCS [mM]
CuSO4 [mM]
3 1 SC 0.05 0.1 1 2
WT
cuf1Δ
cuf1Δ::CUF1-FLAG
ΔKGRP #1
ΔKGRP #2
ΔAce1 #1
ΔAce1 #2
ΔMac1 #1
ΔMac1 #2
cmt1Δ cmt2Δ
ctr1Δ ctr4Δ
C
cuf1Δ::CUF1-FLAG
cuf1Δ
WT Δ181 Δ338 Δ410 Δ513 Δ780
150-
100-
50-
25-
37-
αFLAG-HRP
αGAPDH
SC+ 1mM BCS, 3h, 30°C
SC+ 1mM CuSO4, 3h, 30°C
D
BCS [mM]
CuSO4 [mM]
3 1 SC 0.05 0.1 1 2
WT
cuf1Δ
cuf1Δ::CUF1-FLAG
Δ181
Δ338
Δ410
Δ513
Δ780
cmt1Δ cmt2Δ
ctr1Δ ctr4Δ

Figure 2

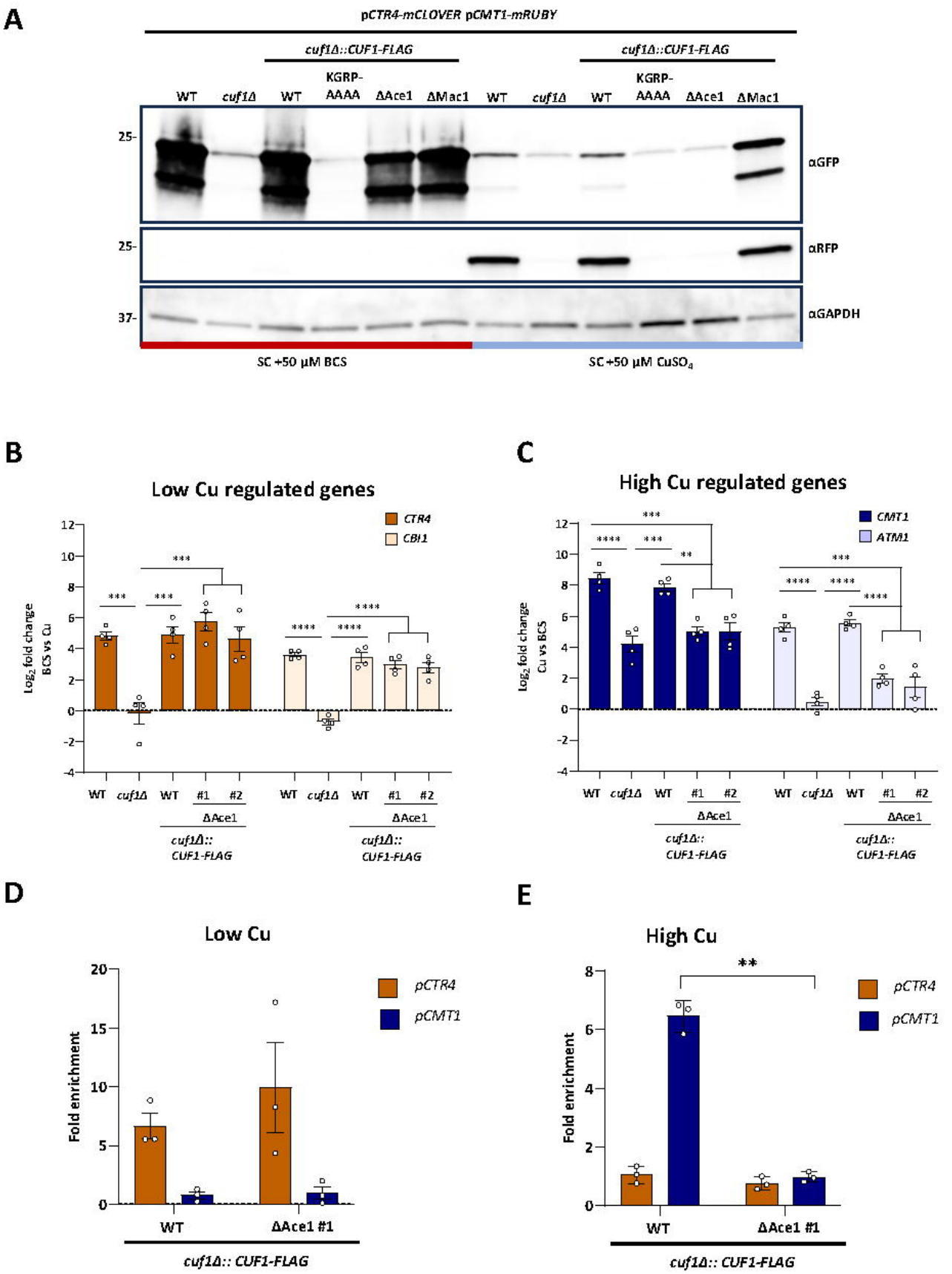
A
pCTR4-mCLOVER pCMT1-mRUBY
cuf1Δ::CUF1-FLAG
cuf1Δ::CUF1-FLAG
WT
cuf1Δ
WT
KGRP-AAAA
ΔAce1
ΔMac1
WT
cuf1Δ
WT
KGRP-AAAA
ΔAce1
ΔMac1
25-
25-
37-
αGFP
αRFP
αGAPDH
SC +50 µM BCS
SC +50 µM CuSO4
B
Low Cu regulated genes
CTR4
CBI1
Log2 fold change BCS vs Cu
WT
cuf1Δ
WT
#1
#2
ΔAce1
cuf1Δ:: CUF1-FLAG
C
High Cu regulated genes
CMT1
ATM1
Log2 fold change Cu vs BCS
D
Low Cu
pCTR4
pCMT1
Fold enrichment
WT
ΔAce1 #1
cuf1Δ:: CUF1-FLAG
E
High Cu
pCTR4
pCMT1
Fold enrichment
WT
ΔAce1 #1
cuf1Δ:: CUF1-FLAG

Figure 3

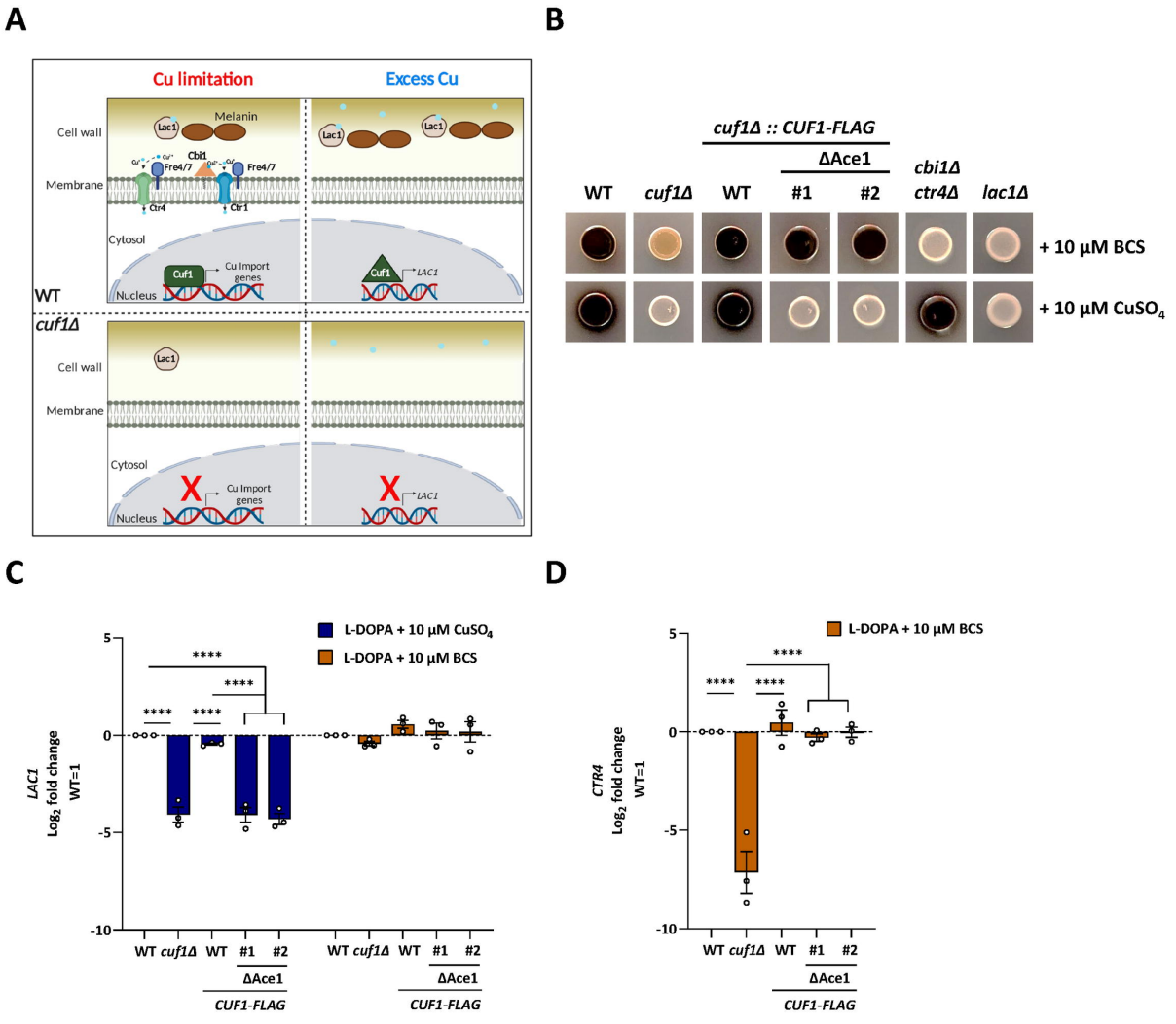
A
Cu limitation
Excess Cu
Cell wall
Melanin
Lac1
Cbi1
Membrane
Fre4/7
Ctr4
Ctr1
Cytosol
Cuf1
Cu Import genes
Nucleus
LAC1
WT
cuf1Δ
B
cuf1Δ :: CUF1-FLAG
ΔAce1
WT
cuf1Δ
#1
#2
cbi1Δ ctr4Δ
lac1Δ
+ 10 µM BCS
+ 10 µM CuSO4
C
L-DOPA + 10 µM CuSO4
L-DOPA + 10 µM BCS
LAC1 Log2 fold change WT=1
****
WT cuf1Δ WT #1 #2
ΔAce1
CUF1-FLAG
D
CTR4 Log2 fold change WT=1

Figure 4

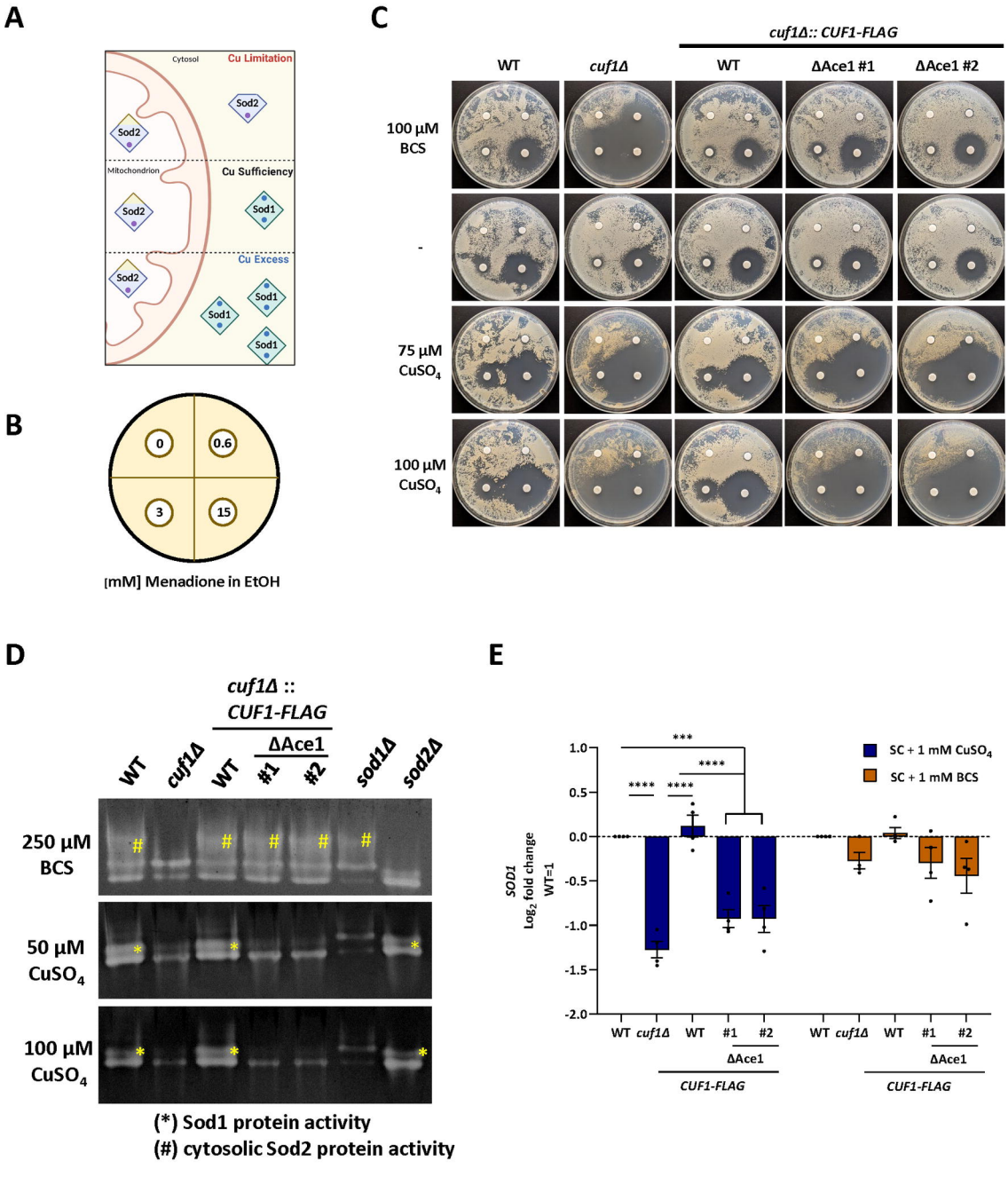
A
Cytosol
Cu Limitation
Sod2
Sod2
Mitochondrion
Cu Sufficiency
Sod2
Sod1
Cu Excess
Sod2
Sod1
Sod1
Sod1
B
0
0.6
3
15
[mM] Menadione in EtOH
C
cuf1Δ:: CUF1-FLAG
WT
cuf1Δ
WT
ΔAce1 #1
ΔAce1 #2
100 µM BCS
-
75 µM CuSO4
100 µM CuSO4
D
cuf1Δ :: CUF1-FLAG
ΔAce1
WT
cuf1Δ
WT
#1
#2
sod1Δ
sod2Δ
250 µM BCS
50 µM CuSO4
100 µM CuSO4
(*) Sod1 protein activity
(#) cytosolic Sod2 protein activity
E
SC + 1 mM CuSO4
SC + 1 mM BCS
SOD1 Log2 fold change WT=1
1.0
0.5
0.0
-0.5
-1.0
-1.5
-2.0
***
****
****
****
WT
cuf1Δ
WT
#1
#2
ΔAce1
CUF1-FLAG
WT
cuf1Δ
WT
#1
#2
ΔAce1
CUF1-FLAG

Figure 5

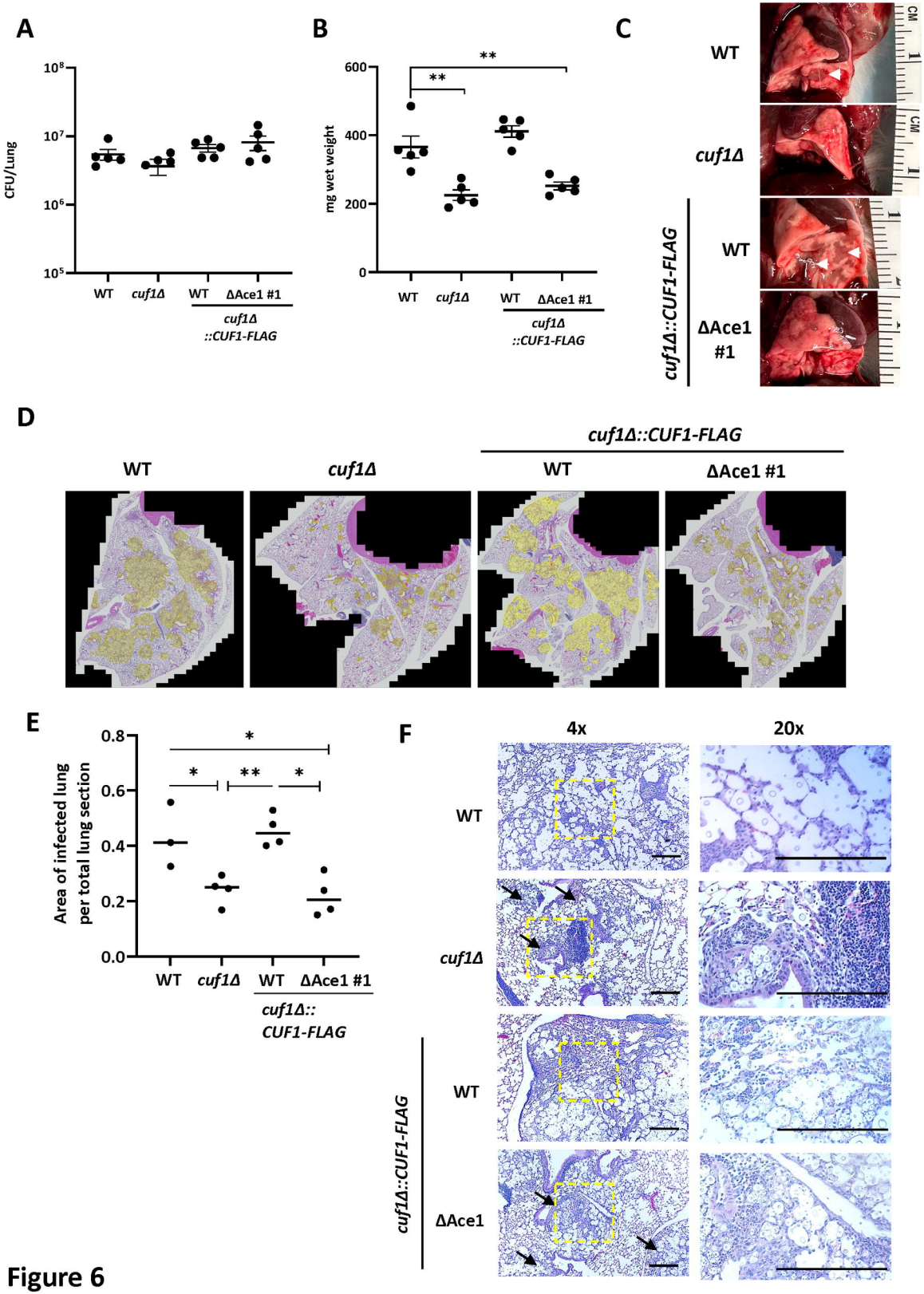
A
CFU/Lung
10^8
10^7
10^6
10^5
WT
cuf1Δ
WT
ΔAce1 #1
cuf1Δ ::CUF1-FLAG
B
mg wet weight
600
400
200
0
**
**
WT
cuf1Δ
WT
ΔAce1 #1
cuf1Δ ::CUF1-FLAG
C
WT
cuf1Δ
cuf1Δ::CUF1-FLAG
WT
ΔAce1 #1
D
cuf1Δ::CUF1-FLAG
WT
cuf1Δ
WT
ΔAce1 #1
E
Area of infected lung per total lung section
0.8
0.6
0.4
0.2
0.0
*
*
**
*
WT
cuf1Δ
WT
ΔAce1 #1
cuf1Δ:: CUF1-FLAG
F
4x
20x
WT
cuf1Δ
cuf1Δ::CUF1-FLAG
WT
ΔAce1

Figure 6